PERGAMON

Journal of Geodynamics 29 (2000) 151–185

JOURNAL OF GEODYNAMICS

Active faulting and earthquake hazard: The case study of the Chihshang Fault, Taiwan

Jacques Angelier[a,*], Hao-Tsu Chu[b], Jian-Cheng Lee[c], Jyr-Ching Hu[c]

[a]*Tectonique Quantitative, Département de Géotectonique and ESA 7072, Université P.-&-M. Curie, Boîte 129, 4 pl. Jussieu, 75252, Paris, Cedex 05, France*
[b]*Central Geological Survey, M.O.E.A., Taipei, Taiwan*
[c]*Institute of Earth Sciences, Academia Sinica, P.O. Box 1-55, Nankang, Taipei, Taiwan*

Abstract

The Longitudinal Valley Fault Zone of eastern Taiwan is the present-day plate boundary between the Philippine Sea Plate and the South China block of Eurasia. Repeated surveys of active deformation were carried out at five sites along its most active segment, the Chihshang Fault. Annual surveys during the period 1990–1997 reveal a rather constant slip velocity of 2.2 cm/yr in a N40°W direction, involving both a thrust component with horizontal shortening of nearly 1.7 cm/yr and a left-lateral component of nearly 1.4 cm/yr. The fault trends N18°E and dips 39–45° to the east. The vertical displacement velocity is about 1.3 cm/yr and the actual oblique offset of the fault increases at a rate of 2.6 cm/yr. Comparison with GPS data suggests that some additional deformation occurs on the edge of the Valley. Active faulting of the Chihshang Fault and of the entire Longitudinal Valley Fault Zone accounts for 24% and 37% (respectively) of the total shortening across the Taiwan collision in the N54°W direction of relative motion between the Philippine Sea Plate and the South China shelf. This distribution of relative displacements illustrates the major role played by this boundary, as a zone of mechanical weakness where tectonic partitioning occurs. Permanent surveying of the displacement on the Chihshang Fault has the potential to detect significant decrease in slip rates, and hence to predict forthcoming locking stages, which would increase earthquake hazard.

* Corresponding author. Fax: +33-1-44-27-50-85.
E-mail address: jacques.angelier@lgs.jussieu.fr (J. Angelier).

0264-3707/00/$ - see front matter
PII: S0264-3707(99)00045-9

1. Introduction

In Taiwan, the main boundary between Eurasia and the Philippine Sea Plate can be observed on land: it is the Longitudinal Valley Fault Zone of eastern Taiwan. This major active fault zone separates two domains that were located at a NW–SE distance of more than 400 km 10 Ma ago. On the western side of the Longitudinal Valley, the Central Range of Taiwan shows a variety of terranes belonging to the continental margin of Eurasia. On the eastern side of the Longitudinal Valley, the Coastal Range is principally composed of calc-alkaline volcanic formations of the northern Luzon arc, late Miocene in age, overlain by thick marine, flysch-like Plio-Quaternary sediments, affected by folding, thrusting and uplift. The importance of the Longitudinal Valley Fault Zone as both a major Late Cenozoic suture zone and the main present-day plate boundary (Fig. 1), was recognized a long time ago by geologists and geophysists working in the area (e.g., Ho, 1986 ; Tsai, 1986).

In this paper, a few aspects of active faulting along this segment of the plate boundary have

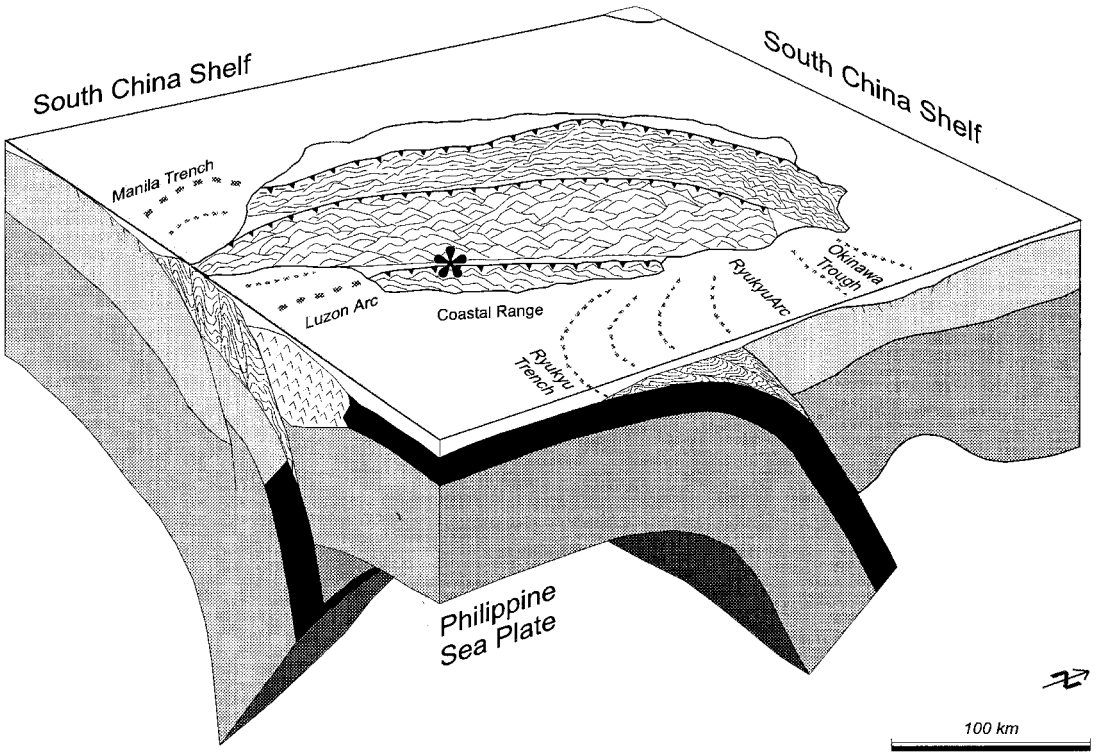

Fig. 1. Schematic view of the Taiwan collision zone. Location of the studied Chihshang Fault, along the Longitudinal Valley Fault Zone, shown as large black asterisk. Note that the Longitudinal Valley Fault Zone is the onland present-day plate boundary between the Philippine Sea plate and Eurasia. Lithospheric pattern of the Taiwan collision zone modified after Angelier (1986). The Taiwan orogen developed between the subduction zones of the Ryukyu arc-and-trench (to the northeast, on right) and the Manila trench–Luzon arc (to the south). Oceanic crust in black, continental crust in medium grey, volcanic island-arc crust with pattern of overturned "v", lithospheric mantle in dark grey and asthenosphere not shown.

been investigated. It is shown that repeated observations in the field may allow one to accurately measure the displacement across the fault zone and to quantify its changes with time. It is also mentioned that these data are significant for earthquake hazard assessment. An earlier study demonstrated that it is possible to obtain reliable annual records of the displacement, based on detailed surveys of partly buried, massive concrete structures at selected sites (Angelier et al., 1997).

2. The longitudinal valley of Taiwan as an active plate boundary

The Longitudinal Valley of eastern Taiwan is a straight, narrow morphological feature separating the high mountains of the Central Range (on the western side) from the Coastal Range (on the eastern side). Both these mountain ranges belong to the collision belt of Taiwan, where fast plate convergence occurs along a SE–NW direction between the Philippine Sea Plate including the Coastal Range and the South China portion of the Eurasian plate, as shown in Fig. 1 (Angelier, 1986). The valley itself is the surface expression of a major lithospheric suture zone extending for more than 160 km along a NNE–SSW direction.

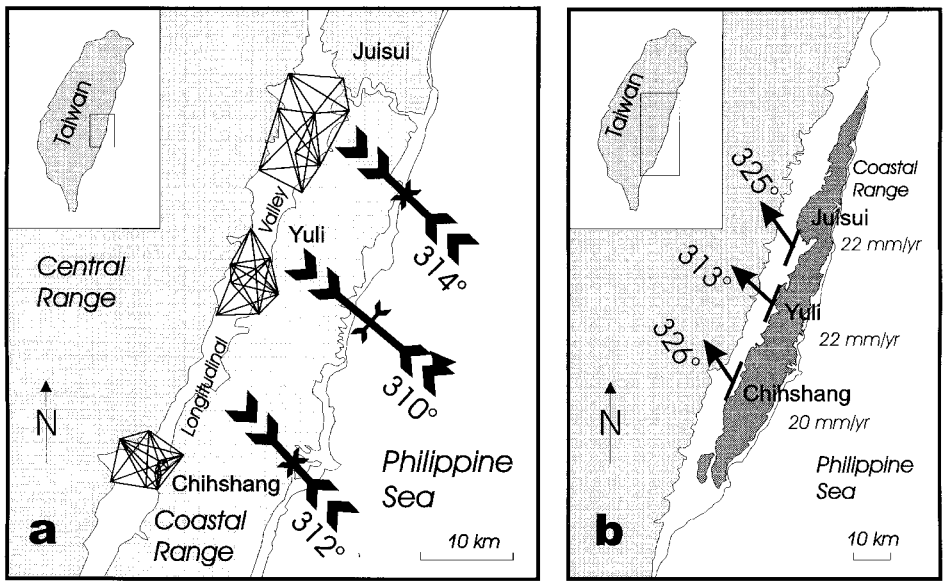

Fig. 2. Deformation and displacement across the Longitudinal Valley Fault Zone, as reconstructed by Lee and Angelier (1993) with the geodetic data from the trilateration networks of Yu and Liu (1989). After Angelier et al. (1997), modified. For geodynamic setting, see Fig. 1. (a) map showing the three geodetic networks (Chihshang, Yuli and Juisui) and the corresponding axes of maximum and minimum shortening (couples of convergent arrows with double and simple arrowheads, respectively, with lengths proportional to principal strain values) obtained after computation of 2-D strain tensors. Azimuths of maximum shortening added. (b) application of models of "discontinuous deformation" (Lee and Angelier, 1993) to the same geodetic networks. Arrows indicate computed displacement of the upthrust, eastern block of the Longitudinal Valley Fault Zone relative to the Central Range. Azimuths of displacement added, in degrees, with computed velocities in mm/yr.

As indicated by the distribution of earthquake foci (e.g., Tsai, 1986), the active shear zone of the Longitudinal Valley strikes N20°E and dips about 45–55° eastwards. This seismic zone is identified from the surface to depths of more than 45 km. Earthquake mechanisms in this zone are reverse and strike-slip in type. They indicate that the motion is oblique, combining reverse faulting (i.e., the thrusting of the Coastal Range towards the northwest, over the Longitudinal Valley) and a minor but significant component of left-lateral strike-slip.

2.1. Fault kinematics reconstructed from local triangulation networks

Geodetic studies have already shown that the present-day deformation across the Longitudinal Valley implies NW–SE horizontal shortening at an average velocity of 2.1 cm/yr. In the late eighties, Yu and Liu (1989) and Yu et al. (1990) established three geodetic networks across the Longitudinal Valley at Chihshang, Yuli and Juisui (the latter two respectively located 23 and 40 km north–northeast of Chihshang, as shown in Fig. 2). Within these networks, repeated geodetic measurements, carried out especially during the period 1983–1988, revealed a rather constant shortening velocity and resulted in well-constrained determinations of relative displacement.

Using two inverse methods (the classical determination of strain tensors and a new search for discontinuities within geodetic networks), Lee and Angelier (1993) re-processed the data published by Yu and Liu (1989). The strain tensor inversions (Fig. 2a) show that the axes of maximum shortening trend Nl32°E (i.e., N48°W) on average, in agreement with the previous determinations. Very similar results were obtained from the three networks, and the deformation rates determined from 1983 to 1988 (based on the data of repeated trilateration surveys) were nearly constant. This consistency in space and time indicates that the kinematic behaviour of a major segment of the Longitudinal Valley Fault was reliably and steadily determined. To these respects, no significant difference was found with the earlier conclusions presented by Yu and Liu (1989).

In addition, Lee and Angelier (1993) carried out the inversion of geodetic data based on a "discontinuous deformation model". The results showed that the relative displacement trends N141°E on average for the same three networks. Within the Chihshang network, it trends N146°E, that is N34°W considering the displacement of the eastern block relative to the western one. This inversion provided very similar estimates of the total displacement for the three networks. It indicated that the eastern side of the Longitudinal Valley moves with a velocity of 2.1 cm/yr on average (consistent with earlier determinations by Yu and Liu (1989), in the N39°W direction relative to the western side (Fig. 2b).

Considering the N18°E trend of the Chihshang Fault, these results of geodetic analyses imply velocity components of 1.8 cm/yr for the transverse (thrust) motion, and 1.1 cm/yr for the left-lateral motion. These estimates deal with the 2-D displacement pattern in the horizontal plane. The 3-D displacement pattern cannot be defined with the trilateration data only and will be discussed later in this paper through additional consideration of the fault attitude including the fault dip.

2.2. Results from satellite geodesy: the Taiwan GPS network

During the last ten years, a systematic geodetic survey of Taiwan and surrounding islands was undertaken by the Institute of Earth Sciences, Academia Sinica, using the Global Positioning System (GPS). The Taiwan GPS network was first established in 1989. The results of the successive surveys were presented by Yu and Chen (1994) and Yu et al. (1995, 1997).

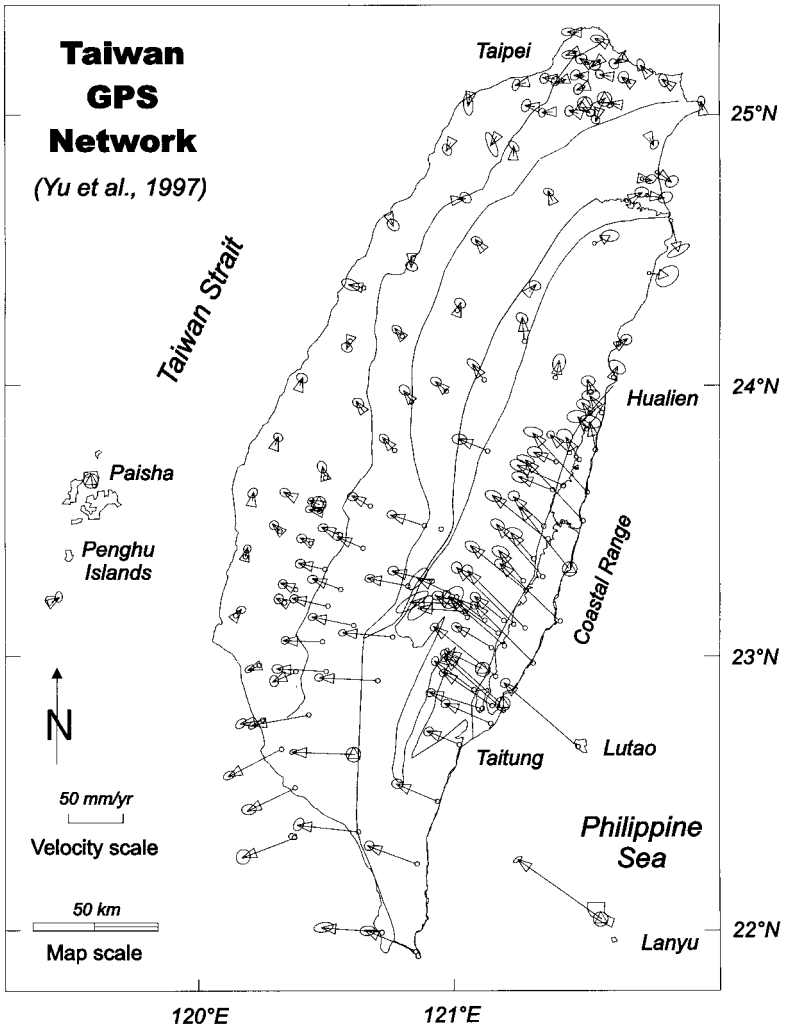

Fig. 3. Map of the velocities of GPS stations in and around Taiwan, slightly modified after Yu et al. (1997). All velocities given relative to the permanent station at Paisha, Penghu Islands, Taiwan Strait, with the azimuth 52,1° between permanent stations Paisha and Taipei fixed. Scale of velocity vectors in lower-left corner of map, in mm/yr. Confidence ellipse (95%) shown at each vector extremity. Network composed of 131 annually surveyed mobile stations and 9 continuously recording stations. Results based on surveys from March 1990 to November 1995. For more explanations, see Yu et al. (1997).

The results used (Fig. 3) were obtained from 9 continuously recording stations and 131 mobile stations annually surveyed from March 1990 to November 1995.

It is necessary to consider first these local results in light of the whole deformation of Taiwan. According to the 1990–1995 GPS velocity field described by Yu et al. (1997), the displacement of the Philippine sea Plate relative to South China occurs in the N54°W direction, with a velocity of 8.2 cm/yr. The westernmost stations of the Taiwan GPS network are located on islands of the continental shelf of the Taiwan Strait, whereas the easternmost stations are located on islands of the northern Luzon arc (Fig. 3). As a consequence, it was possible to measure the relative displacements not only within the deforming collision zone, but also between the stable portions of the Philippine Sea Plate and the South China portion of the Eurasian continent (the Southeast and Northwest corners in Fig. 1, respectively).

The directions of plate convergence near Taiwan, obtained from two independent sources (plate kinematics and GPS studies), are almost the same: 309° and 306° in azimuth (respectively). However, the relative velocity computed by Yu et al. (1997) based on GPS surveying in and around Taiwan, 8.2 cm/yr in the N54°W direction, is significantly larger than that indicated in this region by previous plate kinematics estimates, 7.3 cm/yr in the N51°W direction (Seno, 1977; Seno et al., 1993). This apparent discrepancy principally occurs because the South China shelf (considered in GPS studies, see Fig. 3) is not rigidly attached to Eurasia (considered by Seno). It is reasonable to consider that the islands of the Taiwan Strait considered in the GPS study are rigidly attached to the South China block. Assuming that both determinations were correct, the comparison between the two vectors provides an indirect local estimate, in the Taiwan region, of the eastward displacement of the South China block relative to Eurasia: approximately 1.0 cm/yr in the N77°W direction (Fig. 4).

2.3. Kinematics of the Longitudinal Valley Fault Zone from satellite geodesy (GPS)

Coming back to the Chihshang region, let us consider the GPS data recently published by Yu et al. (1997). We selected five stations of the eastern side of the Longitudinal Valley between 22.88°N and 23.13°N, and five stations of the western side between 22.82°N and 23.11°N (Fig. 3). In the regional frame adopted, the average velocity obtained is 3.3 ± 0.2 cm/

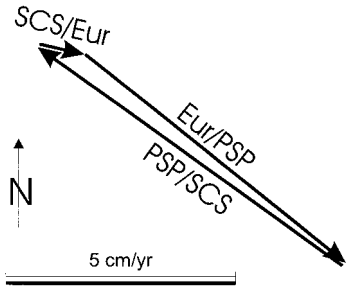

Fig. 4. Velocity triangle showing the relative motions of the Philippine Sea Plate (PSP), Eurasia (Eur) and South China Shelf (SCS), computed in the Taiwan region. Eur/PSP relative displacement based on the determination of Eulerian pole and angular velocity by Seno (1977) and Seno et al. (1993). PSP/SCS relative displacement based on the GPS geodetic studies in and around Taiwan by Yu and Chen (1994) and Yu et al. (1995 and 1997).

yr in the N57°W (± 2°) direction for the five stations to the west (the Central Range side), whereas it is 6.3 ± 0.2 cm/yr in the N47°W (± 2°) direction for the five stations to the east (the Coastal Range side).

Adopting these values and comparing the vectors, one concludes that the velocity of the eastern side relative to the western one averages 3.1 cm/yr in the N37°W direction across the Longitudinal Valley near 23°N. Note that previous estimates based on the earlier GPS data from Yu and Chen (1994) provided somewhat longer but generally similar motion vectors for the western and eastern sides of the Longitudinal Valley : 4.3 cm/yr in the N°59W direction and 6.8 cm/yr in the N°46W direction, respectively (Angelier et al., 1997). The following discussion is based on consideration of the most recent data (3.1 cm/yr and azimuth 143°).

This geometrical reasoning has significant implications. First, across the southern Longitudinal Valley Fault Zone and relative to the N54°W direction of plate convergence, the motion vector of the eastern block is deviated clockwise of 6–7 degrees, whereas that of the western block is deviated counterclockwise of about 3 degrees. In other words, the velocity vectors relative to the South China shelf, which in most cases smoothly vary in orientation across the collision zone (Fig. 3), are abruptly deviated by nearly 10° counterclockwise across the Longitudinal Valley Fault Zone. Considering amplitudes, this change in orientation coincides with a major discontinuity, of about 3 cm/yr, in the velocity field of Taiwan.

At a more local scale, and using the same GPS data, one easily determines the fault slip components along and across the Longitudinal Valley Fault Zone that trends N18°E near Chihshang. The average velocities obtained are 2.5 cm/yr for the reverse transverse component and 1.8 cm/yr for the left-lateral component.

2.4. Contribution of the Longitudinal Valley Fault Zone to plate convergence in Taiwan

The comparison between GPS velocity vectors estimated at regional and local scales in the last two subsections enables one to evaluate the contribution of the Longitudinal Valley Fault Zone in the total deformation across the active collision zone of Taiwan. The local N37°W trend of relative displacement, as compared with the average regional N54°W trend, indicates that the N20°E trending Longitudinal Valley Fault Zone accommodates a higher proportion of left-lateral strike-slip motion than the other units of the Taiwan orogen.

As discussed above, the average shortening velocity across the Longitudinal Valley Fault Zone near 23°N, 3.1 cm/yr in the N37°W direction, has a component of 3 cm/yr along the N54°W direction of convergence. This component, as compared with the velocity of 8.2 cm/yr between the stable blocks on the two sides of the collision zone, indicates that the Longitudinal Valley Fault Zone absorbs more than one third (37%) of the total shortening between the northern Luzon Arc (fixed to the Philippine Sea Plate) and the South China shelf (Fig. 1). For the earlier conventional triangulation networks, the same calculation yields a component of 2.0 cm/yr along the N54°W direction of convergence, that is, about one fourth (24%) of the total shortening. The difference between these values is significant and deserves discussion.

Considering the single segment of the Longitudinal Valley that we are interested in, and taking uncertainties into account, the results of GPS studies indicating an average motion vector oriented N37°W with a velocity of 3.1 cm/yr are fairly compatible with the results of conventional geodesy (yielding a vector oriented N39°W with a velocity of 2.1 cm/yr, as

discussed before). In more detail, however, the velocity computed with the GPS data is almost 1.5 times larger than that calculated within the locals networks, even though the trends do not differ significantly. The WNW–ESE average distance between the two sets of five GPS stations considered is 5.9 km, a distance is in most cases larger than the total width of the earlier local trilateration networks.

The simplest explanation for this apparent discrepancy between the results (3.1 cm/yr for GPS geodesy, as compared with 2.1 cm/yr for previous networks) lies in the probable occurrence of some additional deformation at the mountainous edges of the Longitudinal Valley. Such a deformation should involve oblique, left-lateral shortening very similar in orientation to that of the Longitudinal Valley Fault itself (but with a much smaller magnitude). This inference directly results from the absence of any significant difference between the trends of relative displacement vectors independently determined (N37°W and N39°W as mentioned above). Concerning the location of this inferred deformation, it should obviously be looked for outside, or at the boundary of, the geodetic networks surveyed during the 1983–1988 period. Further geometrical analyses taking into account the accurate locations of the geodetic stations used in both the earlier conventional trilateration and the more recent GPS surveys will confirm, or invalidate, this explanation.

2.5. Belt-parallel and belt-perpendicular kinematics of the Longitudinal Valley Fault Zone

The present-day overall deformation of Taiwan, based on GPS results, can be examined in more detail by distinguishing the transverse and lateral components of the regional deformation in the whole mountain belt (Fig. 3). Taking into account both the general azimuth of plate convergence (126°) and the N20°E average trend of structural grain for the central collision range of Taiwan between 23°N and 24.5°N, one easily determines the contribution of the Longitudinal Valley Fault Zone to the total deformation of the collision zone. One thus obtains very high values : 32% for the across-strike shortening (2.5 cm/yr for a total component of 7.9 cm/yr in the N70°W direction), and 80% for the along-strike displacement (1.8 cm/yr for a total component of 2.3 cm/yr in the left-lateral sense).

This estimation highlights in a simple and demonstrative way the prominent kinematic importance of the Longitudinal Valley Fault Zone in the active Taiwan orogen. A geometrical reasoning based on consideration of present-day deformation revealed by satellite geodesy shows that the present-day oblique faulting in the Longitudinal Valley Fault Zone accounts not only for one third of the total belt-perpendicular shortening, but also for as much as four fifths of the total belt-parallel shear. A 37% contribution of the fault zone in the total, oblique shortening of the Taiwan collision zone was mentioned in the previous subsection. Consideration of belt-parallel and belt-perpendicular components shows that this raw contribution in fact includes contrasting proportions of reverse and strike-slip types. In other words, the contribution of the Longitudinal Valley Fault Zone to left-lateral sliding is 2.5 times larger than its contribution to across-strike shortening.

All these observations confirm that at the Present the Longitudinal Valley Fault Zone is the main kinematic discontinuity in the Taiwan collision belt (Fig. 1), a conclusion also valid for the Quaternary and probably the late Pliocene in view of the geological information available. The presence of this active fault zone is a major source of mechanical weakness, stress–strain

perturbation, and partitioning in the regional deformation field. Accordingly, the sudden deviation of the velocity vectors from the eastern side of the Longitudinal Valley to the western side, nearly 10° counterclockwise as calculated above, is clearly perceptible in the map of Yu et al. (1997) near 23°N–121°E (Fig. 3). Furthermore, recent mechanical analyses based on distinct element numerical modelling revealed the consistency of this behaviour for the major zone of weakness within the general frame of the Taiwan collision (Hu et al., 1997).

In summary, the geodetic analyses of horizontal displacements carried out at different scales, with onland and satellite-based techniques successively, indicate that 37% of the total convergence in the collision zone is absorbed across the Longitudinal Valley, and 24% across the narrow fault zone located on the eastern side of the valley. This corroborates the importance of the Longitudinal Valley Fault Zone as the major active plate boundary, in full agreement with earlier conclusions based on geological evidence and earthquake distribution (e.g., Ho, 1986 and Tsai 1986 respectively). However, as far as the real kinematic behaviour of the active fault at the outcrop scale was concerned, little was known prior to our study in this region.

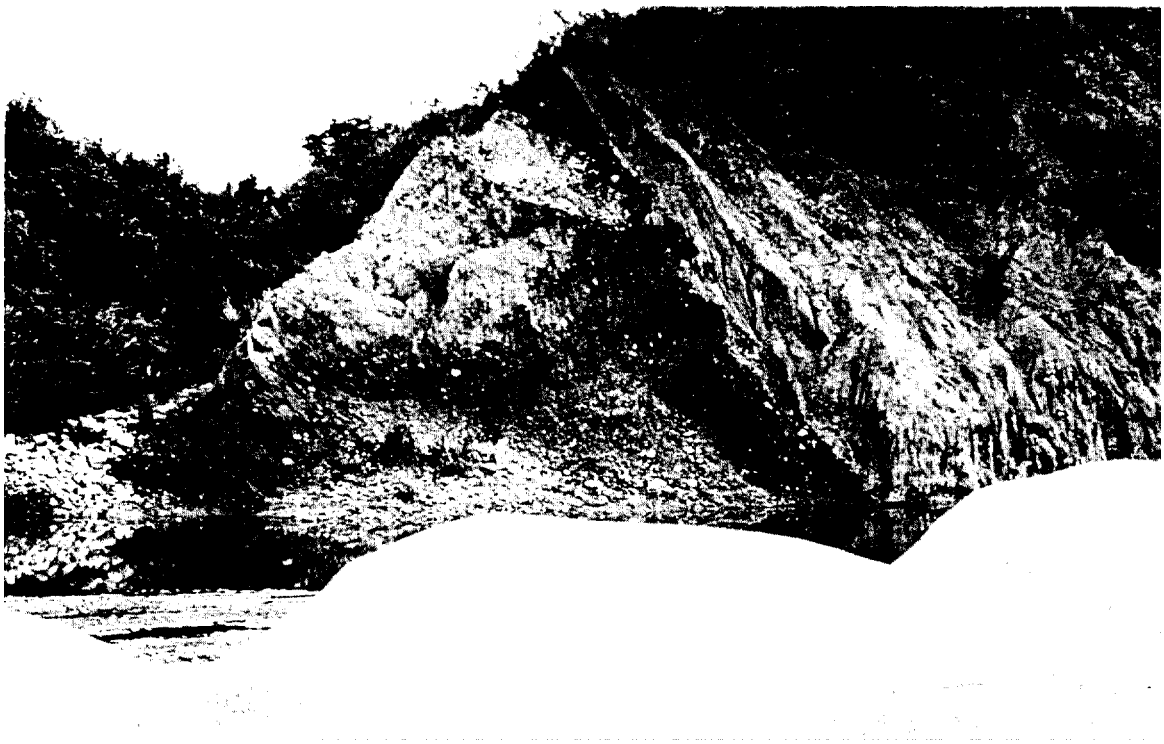

Fig. 5. The Fuli outcrop of the Chihshang Fault. Left side, to the east: Lichi Mélange, Pliocene in age. Right side, to the west: alluvial deposits of the Longitudinal Valley, Quaternary in age. Note the eastward dip of the fault surface, about 45°.

3. Geology and earthquakes along the active Chihshang Fault

In the studied region, a unit of Lichi Mélange separates the formations of the Coastal Range (mainly the Takangkou flysch-like formation of Plio-Pleistocene age, overlying the Tuluanshan calc-alkaline volcanics of the Late Miocene) from the Quaternary continental deposits of the Longitudinal Valley. The Lichi Mélange consists of marine clays, Pliocene in age, containing a variety of blocks, including ophiolitic rocks and Miocene sandstones. The Lichi Mélange is affected by tight folding, extensive shearing, and both west-vergent and east-vergent thrusting, as shown by the analyses of ubiquitous striated shear surfaces.

The trace of the active Chihshang Fault generally follows a major geological contact between the Pliocene Lichi Mélange to the east (on the upthrust side of the fault) and the Pleistocene–Holocene deposits to the west (the Longitudinal Valley, on the downthrown side). The Chihshang Fault generally bounds to the west, but locally cuts through, the Quaternary terraces that uncomformably overlie the Lichi Mélange. These terraces form low flat hills between the bottom of the Longitudinal Valley and the rugged topography of the Coastal Range. Near the village of Fuli, in a valley crossing the fault scarp, the reverse fault surface is exposed, it dips 45° to the east and affects the Lichi Mélange on the eastern, upthrust side and the Quaternary alluvium on the western, downthrown side (Fig. 5).

The Chihshang Fault belongs to the Yuli segment of the Longitudinal Valley. The presence of active faulting in the Longitudinal Valley was recognized a long time ago in the pioneering geological mapping work of Hsu (1962). This was confirmed by geophysical studies revealing high seismic activity (Yu and Tsai, 1982). Earthquakes and active faulting principally occur on the eastern side of the Longitudinal Valley, near the contact with the Coastal Range; they were described by York (1976) and Bonilla (1977). Earthquakes with magnitudes larger than 5 occurred at several places all along the Longitudinal Valley, between Hualien to the north and Taitung to the south. The main events occurred in 1951 (Meilun near Hualien, magnitude Ms = 7.1; Yuli, Ms = 5.3), 1972 (Juisui, Ms = 6.9) and 1986 (Hualien, Ms = 6.4 and 7.8). Large events also occurred prior to 1945, during the Japanese occupation of Taiwan, and before; but they are poorly documented.

Numerous evidences of co-seismic deformation and fracturing in roads, bridges, walls and buildings have also been observed along the Longitudinal Valley Fault Zone. Along the Chihshang Fault, fractures appeared in the ground and buildings in November 1951, during the Taitung earthquakes. However, taking into account the large shortening velocities discussed in the previous section, one would expect more frequent and larger earthquakes to occur in this region. In fact, numerous fractures along the fault zone certainly developed in the absence of significant earthquakes. We obtained this information from inhabitants, based on numerous local inquiries concerning fracture damage that has affected walls, buildings, roads, water channels and other constructions in the Chihshang Fault area. Furthermore, the results of the surveys presented below, as compared with the records of seismicity for the same periods, indicate that most of the fault movement occurred as non-seismic creep, or as progressive slip with minor earthquakes.

4. 3-D records of vertical and horizontal movements

The Chihshang Fault is the southern portion of the Yuli segment of the Longitudinal Valley Fault. It has a length of few tens of kilometres and strikes N18°E. The Chihshang Fault has been active during the last 30 years, as illustrated by fracturing reported at various periods in the roads, walls and buildings along the boundary between the Longitudinal Valley and the Coastal Range.

4.1. The 3-D pattern of slip on the Chihshang Fault

Considering not only the fault location and attitude in outcrops (Fig. 5), but also the results of the geodetic analyses mentioned before, and the distribution of earthquake foci, there is no doubt that near Chihshang a single major fault surface crops out along the eastern boundary of the Longitudinal Valley. Surface studies indicate that this fault trends N18°E and dips about 45° to the east. The distribution of earthquake foci suggests that at depth the fault zone may dip slightly steeper, about 55°. The oblique motion on this fault combines reverse and left-lateral components (Fig. 6). The knowledge of the fault dip allows a three-dimensional understanding of fault kinematics that cannot be reached by the reconstruction of the horizontal deformation only.

Let us consider the angle, α, between the trend (N18°E) and the direction of the relative displacement (N34°W near Chihshang, based on the local geodetic results discussed in an earlier section). The α-value is 52°, and the sense of fault slip is both reverse and left-lateral. With a given fault dip angle, ζ, the three components of the displacement are obtained as function of α and the net horizontal displacement, x. The transverse horizontal displacement (that is, along strike) is $x \sin\alpha$, the longitudinal horizontal displacement (perpendicular to

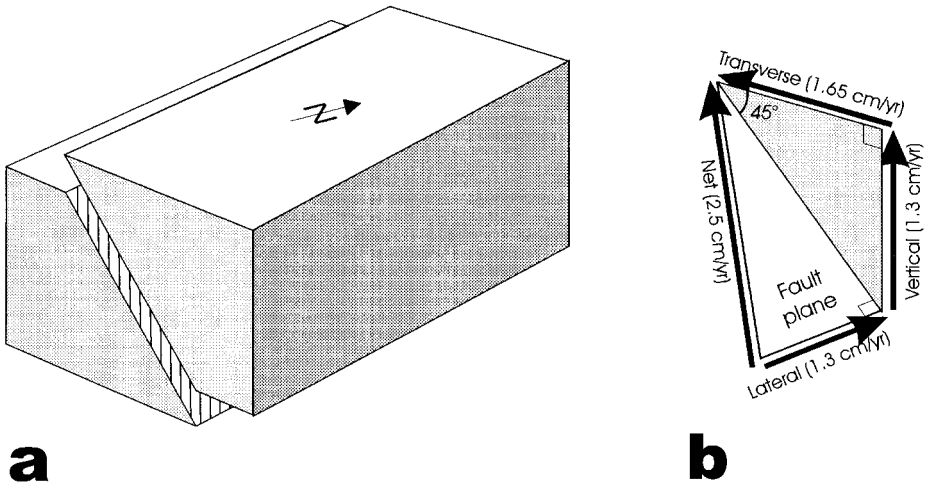

Fig. 6. The three-dimensional behaviour of the Chihshang Fault. (a) illustration of oblique slip, showing the reverse and left-lateral components of motion. (b) quantification of present-day fault slip components, based on consideration of fault geometry (strike and dip) and results of geodetic surveys near Chihshang (discussion in text).

strike) is $x \cos\alpha$, and the vertical offset is $x \cos\alpha \operatorname{tg} \zeta$. A value of 45° is adopted for the fault dip, ζ, as suggested by geological observations and by the distribution of the shallowest earthquakes. The x-value is 2.1 cm (per year), based on the results of the local geodetic studies mentioned before (Fig. 2).

These simple calculations yield average values of 1.65, 1.3 and 1.3 cm/yr for the three components of motion (transverse, lateral and vertical respectively) along the Chihshang Fault. The 3-D pattern of the fault attitude and slip is thus completely reconstructed, with a net slip velocity of 2.5 cm/yr on average (Fig. 6). As shown in the following section, our in-situ measurements along the Chihshang Fault provide slightly larger values (by about 5%); this difference does not substantially affect the 3-D pattern shown in Fig. 6.

Likewise, the estimate of 3-D deformation based on the larger horizontal velocity inferred from GPS studies (with 55° for α and 3.1 cm/yr for x, as discussed earlier), yields values of 2.55, 1.8 and 1.8 cm/yr respectively. The significant difference (roughly 50% more for the GPS-based estimates) can most likely be attributed to the amount of deformation occurring on the edges of the Longitudinal Valley, outside the main fault zone. However, in order to consider these GPS results in the 3-D reconstruction (rather than the results of conventional geodesy), one should assume that in three dimensions this additional deformation is identical in orientation with that observed at the Chihshang Fault. The 2-D aspect in the horizontal plane has been discussed earlier in this paper. Considering the 3-D problem, it appears that if the additional shortening is accommodated by NNE–SSW trending faults, these faults should have approximately the same dips as for the Chihshang Fault. In the absence of relevant geological information, this assumption is far from being demonstrated.

As pointed out before based on comparison between GPS and earlier geodetic results, small

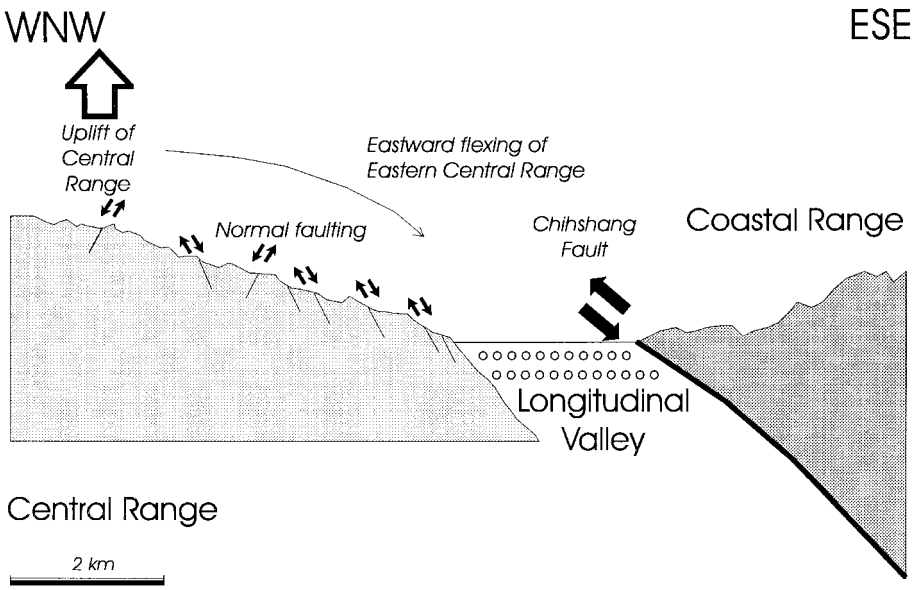

Fig. 7. Schematic interpretative cross-section illustrating the hypothesis of flexing in the eastern Central Range of Taiwan. Couples of arrows show senses of fault movements. See discussion in text.

faults or shear zones probably exist near the edges of the Longitudinal Valley; but their geometry is still unknown. In order to obtain reliable estimates of 3-D deformation, the analysis must be restricted to the well constrained fault displacements. This is not the case for the inferred additional faults which could not be observed yet ; but it is the case for the Chihshang Fault where the slip motion is accurately determined in the field (next section).

It follows that in this case study of active faulting it is better to consider the local geodetic results obtained from conventional geodesy. This is because the local networks allow accurate estimates of horizontal deformation related to this particular fault, whereas the analysis of the GPS data covering a broader area would require risky assumptions on how the additional deformation occurs. We thus constrain our geometrical analysis to the Chihshang Fault itself, which in any case accommodates more than two thirds of the shortening occurring across the whole Longitudinal Valley Fault Zone.

4.2. Insights from vertical motion: the east-Taiwan paradox

The geometrical pattern derived above has strong implications in terms of vertical displacement. In the absence of tilting, the eastern block (the Coastal Range side) should be uplifted at a rate of about 1.3 cm/yr relative to the western one (the Longitudinal Valley and Central Range side), as a simple consequence of the westward thrusting of the Coastal Range over the Longitudinal Valley (Fig. 7).

Near Chihshang, where analyses of trilateration networks during the period 1983–1988 effectively revealed a NW–SE shortening of about 2 cm/yr, geodetic levelling along E-W routes during the period 1986–1988 effectively showed that the western edge of the Coastal Range was uplifted at a rate of about 2 cm/yr, while the Longitudinal Valley was subsiding at a rate of about 1 cm/yr (Yu and Liu, 1989). Thus, these levelling surveys not only revealed the uplift of the eastern block relative to the western one, consistent with the attitude of the active fault, but also showed that the vertical offset observed in 1986–1988 was much larger than that expected according to average velocities (about 3 cm/yr instead of 1–2 cm/yr). However, it is not clear if the present-day estimates of relative motion reflect the behaviour of the fault zone over long time scales.

As a matter of fact, it seem that this possibility is unlikely, because there is strong geological evidence that, during the late Plio-Quaternary collision, the core of the Central Range underwent uplift and erosion with respect to the surrounding domains. On the other hand, it is well known that before colliding against the body of Taiwan the northern Luzon arc suffered strong subsidence. In the Coastal Range, this subsidence is recorded by the Pliocene–early Pleistocene deposition of the thick, deep-marine flysch-like sediments of the Takangkou formation on top of the Late Miocene volcanics, following that of shallow-marine sediments of the Tuluanshan formation. Although this period of subsidence was certainly followed by rapid uplift when the segments of the Luzon arc were accreted and became the Coastal Range, available geological and morphological evidence suggests that stronger uplift has affected the eastern Central Range.

Thus, even in terms of general structural geology, there is a contradiction between the tectonic behaviour of the boundary between the Coastal Range and the Central Range and the Quaternary uplift of the Central Range relative to the Coastal Range (Fig. 7). This is because

the tectonic nature of this boundary, a major west-vergent reverse fault, would imply uplift of the eastern block (the Coastal Range) relative to the western block, which is not the case.

Geological observations seem therefore to indicate that the present-day behaviour of the Longitudinal Valley Fault cannot be extrapolated for long periods in the past. Significant variations with time have certainly affected the response of the Longitudinal Fault Zone to far-field conditions during the last stages of the Taiwan collision. For instance, paleostress analyses indicate that the left-lateral component of relative displacement between the Central Range and the Coastal Range had been larger in the past than during the Quaternary, as compared with the thrust component (Angelier et al., 1986; 1990). Accordingly, one may try to explain the above contradiction in terms of successive contrasting events with different senses of vertical relative displacements. In the studied region studied, this explanation would however contradict most of the geological observations. The east-Taiwan paradox therefore deserves more subtle explanation.

4.3. Thrusting of the Coastal Range and extensional flexing of eastern Central Range

In terms of structural geology, at the scale of several tens of kilometres and few Ma, the apparent major contradiction between the westward thrusting of the Coastal Range and the relative uplift of the Central Range exists only because the westward thrusting of the Coastal Range over the Longitudinal Valley (generally attached to the eastern Central Range) implies its relative uplift. With the thrust dip angle of about 45°, the amounts of relative uplift and shortening should be nearly equal. Not only this is not the case, but also there is geological evidence for a quite significant uplift of the Central Range relative to the Coastal Range at the geological time scale considered.

Geological observation suggests that flexing and normal-type faulting may occur at the regional scale within the eastern Central Range, between the core of the range undergoing strong uplift and the more stable lower slope along the Longitudinal Valley (Fig. 7). At the scale of the collision zone, such a phenomenon is a possible consequence of underplating beneath the Taiwan belt, inducing uplift and arching of the buoyant core of the belt as an isostatic response to thickening and downwarping. Whatever the origin of the phenomenon, the existence of this extensional flexing process is supported by the presence of the Late Cenozoic normal faults cutting the earlier features of the eastern Central Range. It is also supported by the occurrence of present-day earthquakes with normal-type focal mechanisms, beneath the Central Range. This hypothesis of eastward flexing of the whole eastern Central Range (Fig. 7) provides an acceptable geometrical answer to this major challenge in the structural geology of eastern Taiwan, in order to reconcile the contrasting patterns of vertical movements and horizontal deformations.

4.4. Short-term vertical deformation along the fault

Coming back to the local and present-day tectonic scales, the topographic expression of the deformation related to active faulting is illustrated by the presence of an elliptic sagged area near Chihshang. The presence of this depression, which resulted from the deformation of the downthrown block of the major active fault scarp between Tapo and Chihshang, highlights the

recent deformation pattern along the fault zone (Fig. 8). According to local records, this subsidence occurred in 1951, after the Yuli and Taitung earthquakes, and was highlighted by the quick development of swamp areas. Such features are quite visible from topographic maps, aerial photographs and landforms (Lee, 1994). The vertical relative displacement of about 3 cm/yr across the Chishang Fault revealed by levelling studies (Yu and Liu, 1989) is fairly compatible with this spectacular morphological expression.

Interestingly, the location of the Chihshang active fault segment coincides with a zone of relative uplift across the Longitudinal Valley. The topographic high corresponds to a major water divide zone in the drainage network, accentuated by the development of a large alluvial

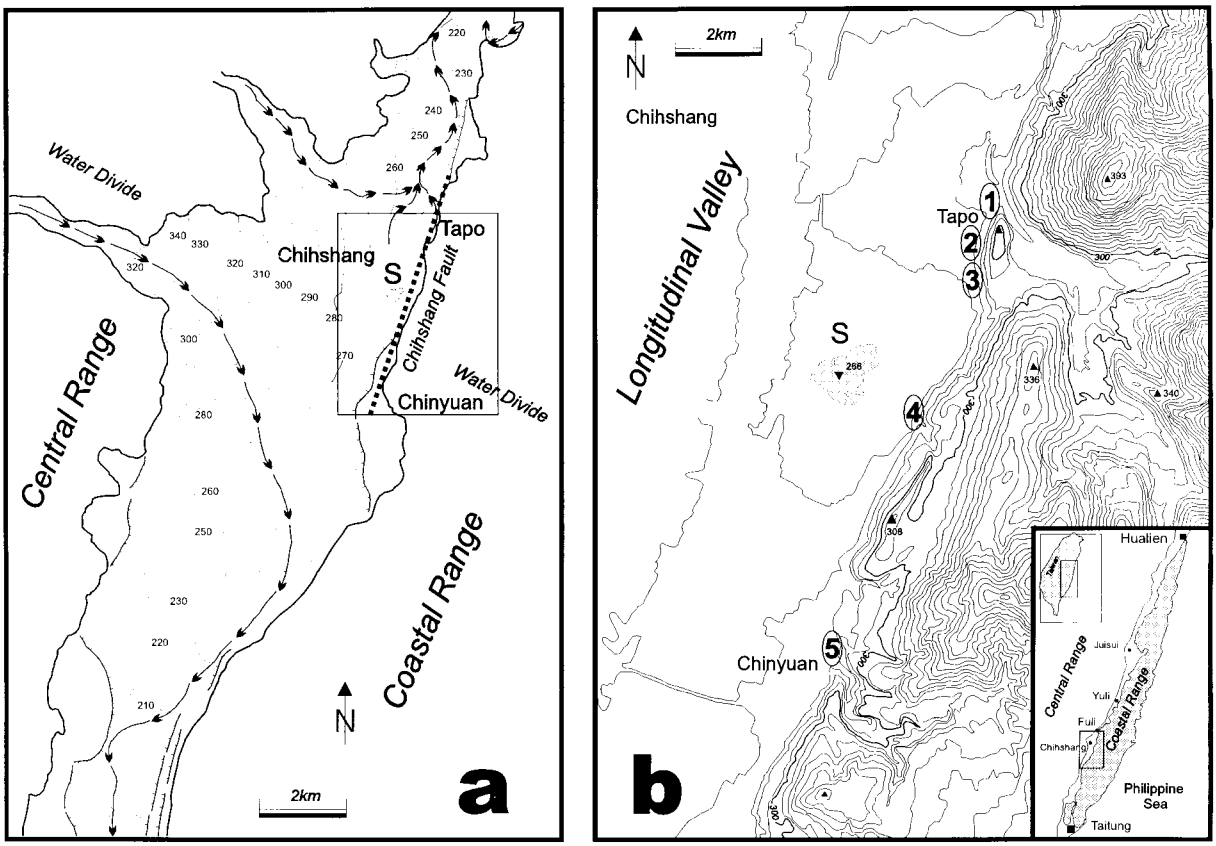

Fig. 8. Morphology of the Chihshang Fault area. Modified after Angelier et al. (1997). General location shown in insert at the lower-right corner of Figure. (a) Topography and drainage pattern of the bottom of the Longitudinal Valley in front of the Chihshang Fault. Elevations in metres (isocontour interval: 10 m), in late quaternary alluvial deposits solely. Main rivers shown as dashed lines with downstream-directed arrows. Note the presence of large alluvial fan and water divide across the valley. Trace of the most active segment of the Chihshang Fault as dotted line. Scarps bounding the quaternary terraces to the west shown as lines (with barbs on the lower side). S, sagged area with swamps that developed in 1951 on the downthrown side of the Chihshang Fault. Rectangular frame: location of area mapped on right. (b) Topography of the Chihshang Fault scarp. Elevations in metres (isocontour interval: 5 m). Villages of Tapo and Chinyuan, and Chihshang city indicated. S, sagged area with swamps (same as in a). Circled numbers 1–5: sites of fault slip measurements mentioned in text.

fan (Fig. 8a). This suggests that near Chihshang the present-day downward motion of the Longitudinal Valley (about 1 cm/yr according to Yu and Liu, 1989) has followed a period of uplift. The compressional deformation of the crust may have concentrated in this area at some period of the Holocene, resulting in the development of a topographic high prior to a major fault break followed by subsidence of the downthrown block in the Longitudinal Valley. Because of the absence of radiometric dating in the coarse alluvial sediments near the Chihshang Fault, the age of this probable reversal in the vertical motion at the local scale is unknown. This interpretation of the recent local evolution in terms of vertical movements influenced by compressive strain and fault breaks not only provides insights for understanding the short-term relationships between horizontal and vertical displacements, but also highlights the poor potential of present-day levelling data to be extrapolated over longer periods of the Quaternary.

5. Active displacement along the Chishang Fault: Site surveying

In this section, we present a summary of our estimates of the present-day displacement across the Chihshang Fault, as revealed by local studies in outcrops. This summary includes both the results of the work done until 1994 (Chu et al., 1994; Angelier et al., 1997) and those of more recent measurements, from 1994 until 1997 (this paper). We analysed the variations of fault motion in space and time, as revealed by frequently repeated surveys, and evaluated the opportunity to use this data set to assess possible variations in earthquake hazard, as a function of changes in fault motion.

5.1. Chronology of surveys

The main sites studied along the Chihshang Fault are numbered 1–5, from north to south. They are located in the map of Fig. 8b. Despite a spectacular expression, the results obtained in site 2, at the Tapo school, should be considered with caution (see next subsection). At all the other sites, annual surveys started in 1990 and included systematic quantification of ongoing fault displacement. Episodic surveys had also been made between 1981 and 1990.

Systematic surveys were carried out from 1990 to 1994 at site 3, from 1993 to 1997 at site 1, from 1990 to 1997 (with an interruption of two years) at site 4, and from 1991 to 1997 at site 5. Our monitoring was interrupted in 1994 at sites 3 and 4, because the concrete structures were destroyed prior to reconstruction as a result of local elections. Fortunately, near Tapo village, detailed surveying at site 1 started in 1993, one year before the destruction at the neighbouring site 3, so that it was possible to correlate the relative displacements between these two sites and to consider surveying at site 1 as a successful continuation of the earlier surveys at site 3. On the contrary, at site 4, between Tapo and Chinyuan (Fig. 8b) a temporal gap in our local records occurred during the period 1994–1995, as a result of the destruction of all benchmarks in 1994. The longest continuous succession of annual surveys was obtained at site 5 in Chinyuan village, where annual measurements were made without interruption for eight years (1990–1997). The data collected at sites 1, 3, 4 and 5 include annual measurements of total fault displacements as well as determination of motion vectors.

5.2. Constraints for selection of measurement sites

There is good evidence of active faulting along the Chihshang Fault. One spectacular case is that of the primary school of the Tapo village (site 2 in Fig. 8b), where concrete stairs fixed to the upthrust block to the east and to the lower block to the west record shortening and steepening along an ESE–WNW direction (Fig. 9). As a simplified way to present this outcrop, one may claim that the top of the stairs is attached to the Philippine Sea Plate (the Coastal Range), whereas the base is attached to Eurasia (the Longitudinal Valley and the Central Range). Measurements at this site reveal both the relative uplift of the eastern side and the horizontal shortening across the fault, with reasonable values as compared with the other results obtained along the Chihshang Fault.

However, if the example of the Tapo school well illustrates fault displacement effects, it cannot be considered fully reliable in terms of fault displacement estimates, even though the calculated values obtained for the average velocity at this site were found to be acceptable. In other words, had this site been the single one along the Chihshang Fault, some doubts might have been raised regarding the significance of observations in terms of fault behaviour and

Fig. 9. The stairs of the Tapo school garden (site 2, location in Fig. 8b). View towards the SE. Note the upflift of the concrete block attached to the upper extremity of concrete stairs, as a response to shortening between Coastal Range (the garden, upstairs) and Longitudinal Valley (downstairs). Note also the concrete reinforcement added in the wall deformed by fault movement. Discussion of significance in text.

velocity estimates. This limitation occurs because fractures affecting constructions above the Earth's surface (buildings and bridges), albeit very useful for detecting active faulting and finding the location of active fault traces, behave in a complex way in response to faulting. Thus, they fail to provide reliable records of relative displacement and deformation. Furthermore, in the case of the Tapo school (Fig. 9), another limitation occurs concerning the reliability of the displacement estimates. This is because local topographic effects and landslide phenomena play a significant, albeit additional, role in the slope of the hill adjacent to the school. For these reasons, and despite their numerical consistency with measurements at the other sites, the results obtained at site 1 were not included in the graph of Fig. 10.

In contrast, massive concrete walls are present beneath the ground surface in relatively flat areas along roads and water channels. They were used as bench-marks in local analyses to quantify the displacement across the Chihshang Fault. Because of their strong mechanical coupling with the ground, they provide reliable local records of the amounts of fault displacement, as far as sites with slope instability are not included in the analysis. Along the Chihshang Fault, only four sites (Fig. 8) matched the appropriate requirements, and thus were extensively and repeatedly analysed.

A complete account of the measurements made from 1982 to 1994 at sites 3, 4 and 5 was

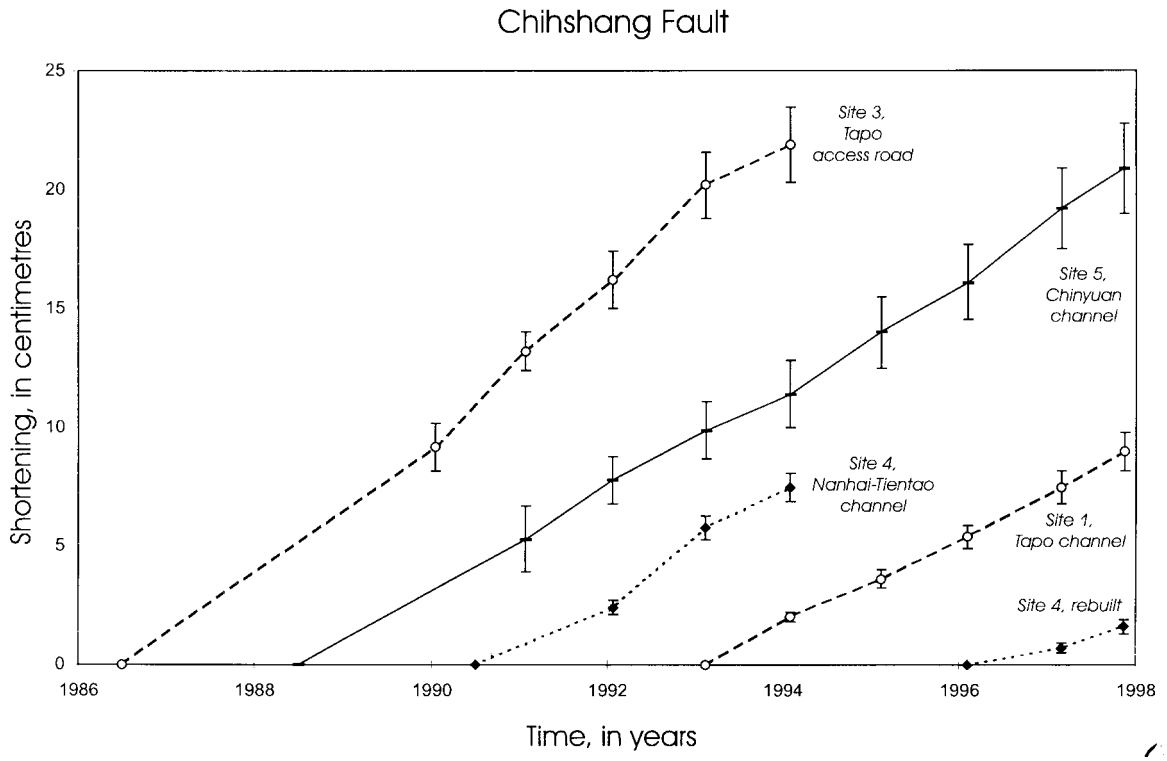

Fig. 10. The evolution of shortening across the Chihshang Fault, as indicated by annual surveys at sites 1, 3, 4 and 5 (location in Fig. 8b). Shortening measured along the trend of relative motion vector. Cumulative displacement since wall construction as ordinate, time as abscissa. Average values as dots, error bars added.

presented in an earlier paper, where the details of the fault displacement geometry until 1994 were also given (Angelier et al., 1997). The observations made at site 1 and those made later than 1994 at all sites, described in the present paper, follow the same principles. Starting in 1982, local enquiries were also done in order to know when the walls were built. The initial construction dates were thus known at the three sites, with an accuracy of one year or better. The periods of later destruction and re-building of the walls were accurately known. The graph of Fig. 10 summarises our measurements of deformation from 1986 to 1997.

5.3. Fault shortening measurements: techniques

The techniques that we adopted until 1994 to determine fault displacements have been presented elsewhere (Angelier et al., 1997). Pre-existing benchmarks, such as stones in concrete, wall crests and drainage pipes were extensively used, especially during the first steps of our surveying. Particular attention was given to the three-dimensional determination of motion vectors. Accurate and reliable estimates of vector orientations and amplitudes were also obtained by matching irregularities on both sides of faults (zig-zag patterns on fracture rims and displacement of stones relative to their inprints on the opposite side). Strong preference was given to measurements done near the base of the walls (because wall base generally undergoes little or no displacement relative to the ground, contrary to wall top), and across isolated faults (because measurements across complex fracture arrays generally involve larger uncertainties).

At sites 1, 3, 4 and 5, and from 1992 to 1997, the techniques that we adopted for fault displacement estimates included an increasing proportion of measurements in nail networks set up in all sites at the decametric to hectometric scales. This technical change occurred in response to the need for better accuracy in length measurements, relative to the simple consideration of natural benchmarks involved in the earlier work. It also fulfilled the requirement for large numbers of regularly spaced control points in grids. Using nail heads as benchmarks effectively resulted in a better accuracy (about half a millimetre for the most usual distances of 2–3 m between nails). The reliability was also better, resulting not only from a better definition of nodes within each network but also from the combination of internal geometrical constraints within the grids (according to triangulation methods).

Because our networks were made of solid figures (adjacent triangles, or quadrangles with diagonals forming partly superposed triangles), it became possible to reconstruct the deformation in the wall plane through determination of horizontal and dip-slip components. However, because the height of the walls remained limited (1–3 m depending on the site), most networks had long and narrow shapes, so that the uncertainties concerning the vertical components of deformation remained large while the horizontal components in the grid plane were determined with increasing accuracy. The nail networks were established not only in the concrete walls but also in horizontal surfaces, in order to allow 3-D reconstitution of fault slip. As compared with the previous use of natural benchmarks, such new data collection was much less dependent on local damage along fractures and faults, the accuracy at each site averaging 0.2–0.3 cm. As a counterpart, such measurements of incremental deformation by essence did not provide estimates of total displacement since wall construction and fracturing.

Summarising, we used two main groups of techniques until 1997. The local collection of 3-D

displacement data along fractures and faults have no capacity to account for deformation within the blocks. In contrast, the collection of length data along lines of benchmarks (1-D) or within nail networks (2-D) may allow detection of deformation even in the absence of macroscopic fracturing. In fact, it revealed that at all sites along the Chihshang Fault the internal deformation of the blocks on both sides of a fracture is negligible (that is, throughout successive surveys, the differences in the measured lengths between the faults remained smaller than the uncertainties). Finally, by combining these different data, we had the opportunity to completely reconstruct the 3-D displacement and deformation patterns.

5.4. Measurement sites and surveying along the Chihshang Fault

The results of our surveys are summarized in Fig. 10, where the estimates of increasing shortening across the Chihshang Fault and the related uncertainties, as obtained at sites 1, 3, 4 and 5, are plotted from 1986 to late 1997. Until 1990 (site 3), 1991 (site 5) or 1992 (site 4), the estimates were based on our knowledge of construction dates and observation of the total displacements affecting pre-existing benchmarks. For these periods, the shortening velocity is

Fig. 11. The faulted wall of the Tapo access road, southwestern entrance of Tapo village (site 3, location in Fig. 8b). SSE on right side. Wall built in early 1984, striking NNW–SSE and facing west, 1.8–1.85 m high. Note the presence of the two reverse faults mentioned in text. Upper fault developed in 1986, lower fault developed in 1989.

simply extrapolated, from the time of initial fracturing and faulting in walls to the time of our earliest length measurement. For the following periods, the displacement estimates combined measurements of total deformation and measurements of annual incremental deformation, resulting in higher accuracy (Fig. 10).

At site 1, along the Tapo River channel, the fault displacement was recorded in concrete dykes on both sides of the river that crosses the active fault north of Tapo. At site 3, along the Tapo access road (Fig. 11, location in Fig. 8b), concrete walls offset by the reverse fault were observed as soon as in 1981 (Barrier and Chu, 1984). Unfortunately, no displacement estimate was done until the damaged wall was destroyed and rebuilt in 1984. The main wall, facing west and approximately 90 m long, trends NNW–SSE. En-échelon fractures developed and became observable in 1986, as an expression of continuing reverse faulting. For interpolation of fault shortening until 1990 at site 3 (Fig. 10), we adopted this 1986 stage rather then the 1984 construction. This was because the latter history (after 1994) showed that prior to fracturing in a new wall the deformation occurred through tilting and warping processes, hence did not contribute to the total variation of wall length measured at subsequent stages.

At site 3, the reverse fault in the wall was well-developed in 1988. In 1989–1990, a second reverse fault appeared 9.5 m west of the older one. Interestingly, the second fault developed at

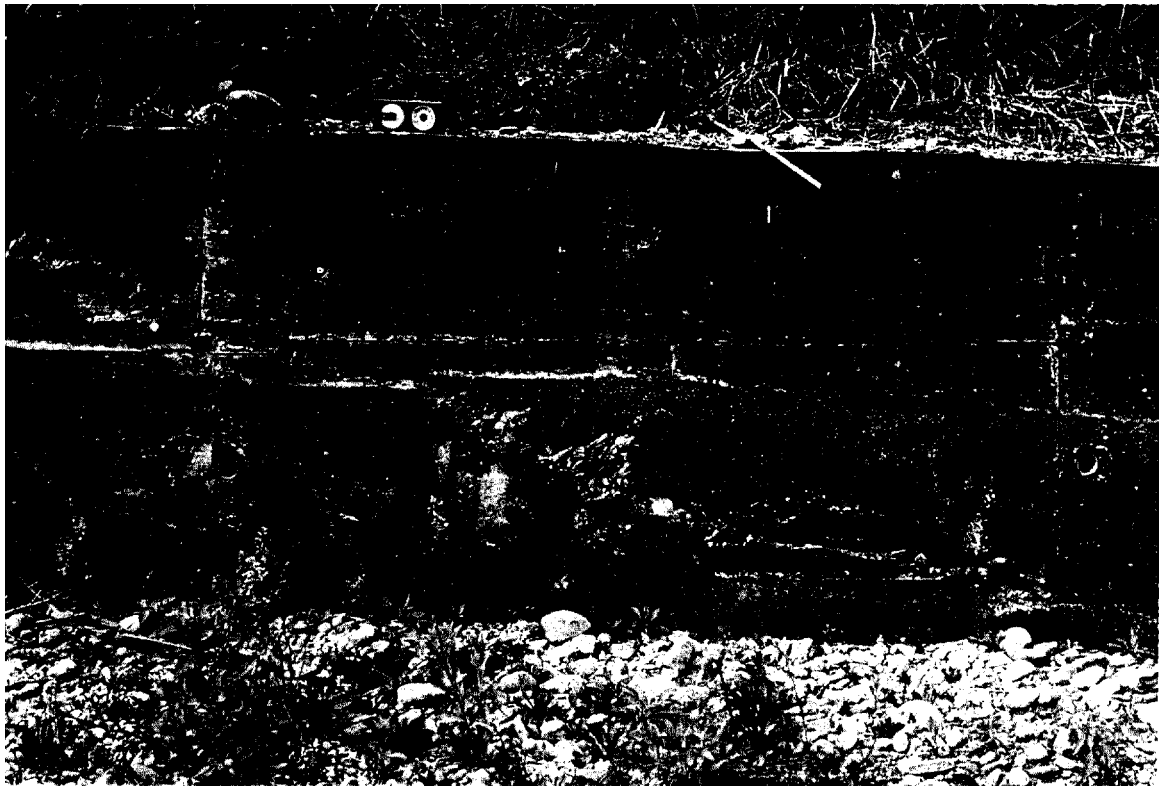

Fig. 12. Reverse fault at Nanhai–Tientao (site 4 between Tapo and Chinyuan, location in Fig. 8b). Southern side of the channel. WNW on right side. Wall built in 1987–1990, striking WNW–ESE and facing north, and 1.5 m high. Note the westward dip of fault in the wall, opposite to the dip of the Chihshang Fault, as discussed in text.

a lower location (Fig. 11), as it is often observed for in-sequence thrusts in sandbox experiments, or reconstructed through stratigraphic dating of thrust movements in mountain belts. The offset of both these reverse faults increased from 1990 to 1994. Consistent with the succession of the two faults, the reverse slip on the upper fault decreased progressively after the development of the lower one, so that the lower fault accommodated an increasing proportion of the total displacement (detailed records in Angelier et al., 1997). In 1992, most of the displacement at site 3 took place on the lower fault.

In 1994, the wall was destroyed and rebuilt at site 3. During the next three years, the deformation of the new wall could not be measured with the techniques that we used at that time. The along-strike deformation remained non-significant. Because other sites revealed continuing activity of the fault (Fig. 10), we inferred that deformation at site 3 involved tilting and warping rather than fracturing and faulting, as a result of massive concrete wall design precluding quick brittle response to shortening. Geodetic levelling, which had the potential to quantify such deformation in the fault zone, was not undertaken.

At site 4, near the Nanhai Tientao temple between Tapo and Chihshang (Fig. 12, location in

Fig. 13. The upper reverse fault in the Chinyuan channel, upstream subsite (site 5, northern Chinyuan village, location in Fig. 8b). Eastern side of the channel. SSE on right side. Wall built in 1984–1985, striking NNW–SSE and facing west, and 2–2.5 m high. Note that the reverse fault locally developed horizontally along a weak zone of aligned water drainage pipes in the wall. Note also that the fault ends to the left in a triangular zone, as discussed in text.

Fig. 8b), the Chihshang fault crosses at nearly right angle the WNW–ESE trending concrete walls, more than 100 m long, of a WNW–ESE drainage channel across the active faults between the villages of Tapo and Chinyuan. The interest of this site lies not only in this near-perpendicular relationship between the fault trace and the walls used as benchmarks, but also in the ground flatness at the fault location. After the construction of concrete channel walls in 1987–1990, N–S fractures developed, and could be observed, since 1990–1991. An east-vergent reverse fault developed in 1991–1992 in the concrete walls. This fault (Fig. 12) represents the surface expression of the main reverse fault, which is west-vergent. This resembles the classical triangular pattern often observed in sandbox shortening experiments, or reconstructed from subsurface observations at mountain belt fronts.

The channel at site 4 was partly destroyed and rebuilt in 1994. Interestingly, no deformation occurred from 1994 to 1997 within the segment rebuilt (west of the road between Tapo and Chinyuan). The brittle deformation developed in the segment previously left intact by fracturing and faulting, east of the road. The probable cause of this eastward shift of the fault at the surface was the better quality and larger thickness of the concrete used in the walls built in 1994, as compared with the earlier ones. As a result, fracturing and faulting required less energy to develop in the old wall than in the new one, despite the energy required to propagate eastward the uppermost section of the fault (of about 10–20 m).

Why did this mechanical response differ from that in site 3, where no fracturing was still observable 3–4 years after wall reconstruction? This was probably because at site 4 a portion of the concrete channel close to the fault was not rebuilt, thus offering a mechanically weaker segment where subsequent shortening could concentrate. As mentioned above, the wall at site 3, approximately 90 m long, had been entirely rebuilt in thick resistant concrete on both sides of the fault trace, so that no particular weakness zone was remaining at the surface above the fault; as a consequence, the compressional strain developing since construction in 1994 was still not large enough to induce fracturing in 1997.

The site 5 is located in the village of Chinyuan (Fig. 13, location in Fig. 8b), where concrete dykes on both sides of the river cross several branches of the active fault, defining three main subsites. The two main advantages of this site lie in the existence of a large flat area affected by the Chihshang Fault (as for site 4, and contrary to site 3) and in the absence of any destruction since wall construction in 1984–1985. As a result, annual surveying could be done without any interruption from 1991 to 1997 (Fig. 10). On the other hand, surveying was more complex at site 5 because in Chinyuan the Chihshang Fault includes several branches, so that it was necessary to carry out measurements of fault displacement at 3–4 subsites.

The easternmost subsites of site 5 are located upstream in the Chinyuan river, with both channel walls (trending NNW–SSE) oblique to the traces of the upper and intermediate branches of the fault that trend NNE–SSW (Fig. 13). Another subsite near the northern entrance of the Chinyuan village coincides with a bend of the river. Thus, the variable angles between the channel axis and the trace of the lower branch of the fault result in a complex distribution of fracturing in the channel walls. Downstream, near the northwest entrance of Chinyuan, an additional subsite shows incipient fracturing, hence revealing the probable development of a new, lowermost fault to the west. However, the deformation is still negligible at this location.

In the Chinyuan village, numerous offsets affect walls, houses and farms in a rather

spectacular way, as a result of active faulting. However, they generally fail to provide reliable quantification of the deformation. All reliable displacement estimates were obtained along the river walls, at the three main subsites of site 5. In this locality, three main fracture zones, with horizontal spacings of 40 and 15 m, developed as the upper, intermediate and middle branches of the Chihshang Fault. As mentioned above, fractures were also noticed in 1992 at a distance of about 200 m downstream, suggesting that a fourth, lowermost fault branch will soon develop there. This phenomenon of in-sequence faulting resembles that observed at site 3, but the scale is 20 times larger in Chinyuan than in Tapo.

In contrast with all the other sites, where no significant deformation could be observed on both sides of the narrow fault zone, site 5 reveals that the Chihshang Fault may locally split into branches. It was thus necessary to measure first the displacements across the different fault branches of the fault (Angelier et al., 1997), and then to add the corresponding motion vectors in order to obtain the estimates of the total fault motion (Fig. 10).

6. Fault attitude and orientation of fault displacements

Relative displacement vectors could be reconstructed in a reliable way from 1986 to 1997, at three of the four sites examined (3, 4 and 5; location in Fig. 8b). No significant variation with time was noticed in the orientation of these vectors.

6.1. Local determination of motion vectors and reliability of data

Using the techniques discussed before, fifteen motion vectors were measured in 1990–1994 at site 3 (Tapo access road, Fig. 11). These vectors trend N156°E and plunge 36°S. The fault trace (N23°E) makes a relatively small angle (about 45°) with the wall trend. Because of this obliquity, the behaviour of the broken wall may be influenced by the lateral pressure of terranes, in such a way that the horizontal component of displacement perpendicular to wall strike increases, relative to that induced by the sole displacement of the fault at depth.

Can the effect of wall-fault obliquity on the validity of the results be estimated? This is an important problem because the determination of fault motion vectors may be significantly, albeit slightly, influenced by the deviatoric effect of the absence of earth on one side of a wall. The answer was partly obtained at site 4 (Fig. 12), where the symmetry between the two concrete walls crosscut at right angle by the fault allowed a rigorous comparison between the two motion vectors which, in fact, are identical in amplitude, but differ slightly in orientation. Relative to the N121°E trend of the channel, the trends of motion vectors on the northern and southern rims make angles of 13° clockwise and 17° counterclockwise, respectively. This difference shows that while the active fault moves, a minor but significant additional displacement of the upper block occurs towards the free axis of the channel, as a consequence of the pressure exerted by the adjacent terranes on the fractured walls. The rigidity of buried concrete walls diminishes when fracturing occurs, thus explaining why these symmetrical across-strike components (which had no expression prior to fracturing) may induce minor deformation after fault development. The deviation occurs in such a way that the additional

component of motion of the upper block relative to the lower block is directed towards the free side of the wall.

In the case of site 4, this deviation averaged 15° near the top of the concrete walls, a rather high value. Adopting the same value at site 3 would suggest a N171°E trend for the average motion vector, hence a larger component of strike-slip, compared with the N156°E trend effectively measured. However, the observations carried out at site 3 revealed that the across-strike displacement of the wall was not much, indicating that the action of ground pressure there did not induce large perturbation in the measured motion vector relative to that of the deeper fault. We conclude that the results obtained at site 4 should not be extrapolated at site 3. Therefore, the N156°E trend of fault motion vector directly measured at site 3 is more reliable than that of the corrected value.

The opportunity to determine perturbations related to ground pressure on both sides of the faulted channel allowed accurate corrections to be made at site 4, resulting in a good determination of six motion vectors from 1992 to 1994, with an average trend N119°E for the period 1991–1994. Furthermore, the plunges (42° on average) are also consistent. The interest of this site therefore results not only from the symmetry of the channel, but also from its orientation nearly perpendicular to the active fault trace. In contrast, the trends significantly differ depending on the channel side. Because at this site uncertainties are less than $\pm 5°$ for both the trend and the plunge, the determinations of motion vectors there are the most accurate data available along the Chihshang Fault.

In the upstream subsite of the site number 5 (Fig. 13), the geometrical relationship between wall strike, fault strike and motion vector trend resembles that observed at site 3. As discussed by Angelier et al. (1997), the best observations were obtained at sites where the angle between the wall trend and the fault trace is close either to 90° or to 0°. This is because at the other sites, with oblique angles (30° to 60°), the deformation involves more complex fracturing and in some cases rotations of wall segments, so that reliable reconstruction of displacement is difficult to obtain.

The motion vectors measured at site 5 (upper fault subsite) also resemble those observed at site 3, with consistent average values: N155°E for the trend and 27° for the plunge. Although uncertainties are larger than in the case previously discussed, the orientation of the motion vectors measured in the walls for the middle fault is similar. Accurate data, however, could be obtained from a nearly horizontal nail network installed in the flat, concrete bottom of the channel (middle fault subsite). The geometrical analysis of the results indicates a N135°E trend for the relative displacement across the reverse fault. Based on determinations of motion vectors for these two fault branches, the average trend of motion vector at site 5 is close to N145°E.

6.2. Geometry of slip along the Chihshang Fault

Comparing the results obtained at sites 3, 4 and 5, and remembering that the trace of the Chihshang Fault is straight and strikes N18°E (Fig. 8), one concludes that the average relative motion vector trends N40°W, that is, oblique to the fault trace at an angle of 58°. This suggests that the left-lateral and the transverse components represent 38% and 62% of the horizontal displacement respectively.

The plunge of motion vectors falls in the range 27–42°. Considering realistic uncertainties which may reach 10–20° for plunges, the local values are not significantly different. This poor accuracy results principally from the elongated shape of nail networks on concrete walls, and from the absence of levelling studies. Moreover, the steepest plunges measured (42°) are consistent with the geological and geophysical information concerning fault attitude. The lowest bound (27°) is consistent with the probable flattening of the reverse fault near the ground surface. Because fracture zones in concrete walls behave as reverse faults with a component of vertical opening, the dips of the fractures themselves have little interest whereas the plunges of motion vectors (steeper than the dips of open fractures) reveal the deeper fault geometry.

Before wall destruction in 1994, the apparent dip direction of the reverse fault at site 4 was opposite to that observed at other sites. This intriguing reversal probably results from the existence of a local triangular zone, as mentioned before, and/or from accommodation of fault slip associated with strain release in the frontal of the earlier maximum downwarping. The second hypothesis is supported by the presence, near site 4, of the sagged area that developed in 1951 after the earthquake crisis (Fig. 8). Furthermore, the deformation zone was shifted of about 10 m to the west after wall destruction and reconstruction in 1994 at site 4, and the new fracture pattern revealed an eastward plunge of the reverse fault, as for the other sites.

In terms of trend, the values obtained at Tapo and Chinyuan are similar (N30°W on average), whereas those of site 4 (N61°W on average) show a deviation as large as about 30° counterclockwise. The difference is three times larger than the realistic uncertainties for our trend estimates (less than 10°–12°). Such a discrepancy is therefore far beyond the range of uncertainties and should be considered geologically significant. It also suggests that relative to the transverse component of slip, the strike-slip component of slip is larger near the tips of the active fault segment (sites 3 and 5) than in its middle portion (site 4). Near the tips, the obliquity between fault trace and motion trend averages 48°, so that the transverse slip (reverse) and the lateral slip (sinistral) are almost equal (53% and 47% of the horizontal slip, respectively). In contrast, near the centre, this angle is about 80° (79° at site 4), and hence the transverse slip can be much larger than the lateral slip (84% and 16% of the net horizontal slip, respectively).

7. Average velocities of slip along the Chihshang Fault

Our determinations at the four sites examined (1, 3, 4 and 5; Fig. 8) provide consistent estimates of the amounts of shortening from 1986 to 1997, and shortening velocities averaged for periods of approximately one year since 1990 (Fig. 10).

7.1. Summary of velocity data, 1986–1997

At site 3, a total shortening of 21.9 cm was measured for a period of about 8 years, in the wall built in 1984. The deformation observed began with the first en échelon fracturing in 1986, and continued with reverse faulting until wall destruction in 1994 (Fig. 10). Successive estimates of total shortening revealed that, within the range of uncertainties, the increase in

total shortening was nearly linear during the period 1990–1993 (before 1990, surveys were few). Because of technical improvement, the annual determinations of shortening were more accurate in 1992–1994. The total motion slightly diminished in 1994. Similar average rates of shortening, 2.7 cm/yr, were computed for the periods 1986–1989 and 1990–1994 (Fig. 10).

After a new wall was built at site 3 in 1994, accurate surveys were done once or twice a year. They revealed the absence of significant shortening from 1994 to 1997. The shortening across the active fault is continuing in this area, as revealed at neighbouring sites. It is likely that at site 3 the shortening is being temporarily accommodated near the wall tips (in the soft ground where no accurate records can be obtained), and also absorbed by tilting or bending of the whole wall (a phenomenon that could not be recorded in the absence of levelling analyses). This change in the deformation mode resulted from the mechanical properties of the wall built in 1994, which is higher, thicker and more resistant than the previous one.

At site 3, a probable scenario for the next future involves fracturing close to the previous location of the fault, followed by reverse offset as in the past. Fracturing is expected to occur when the processes presently active (shortening at wall tips and overall bending-tilting) will become unable to accommodate the increasing shortening. The previous history of this site suggests that a period of 2–4 years of ongoing shortening is required before fracturing, but in the case of the wall built in 1994 the delay may be longer as a result of better construction, resulting in more resistant concrete features overlying the soft terranes of the Pliocene Lichi Mélange and the Quaternary fluviatile deposits. A shift of the emergent portion of the fault zone by few tens of metres cannot however be excluded, depending on the balance between the energy required to break the rigid wall above the fault and that necessary for creating a new shear fracture running in soft formations towards the wall tips. Such a phenomenon is illustrated in the faulting history at the next site to the south.

At site 4, the first data collection was made in 1992, giving the total displacement since the channel construction and fracturing. The next surveys were made in 1993 and 1994. The data revealed a velocity of 2.1 cm /yr for horizontal shortening, resulting in a total displacement of 7.5 cm in about 3.5 years (1990–1994). The wall was destroyed and re-built in 1994, which resulted in a gap in our surveys (Fig. 10). Furthermore, the location of the main zone of deformation changed, as a probable consequence of contrasts in wall quality (the newly built channel segment being more rigid). The phenomenon resembles that expected at site 3, but the deformation could be soon monitored again at the new location in site 4, which was not the case at Tapo where no relatively weak wall segment was subsisting in late 1994. After an intermediate period of progressive fracturing in 1996, the horizontal shortening velocity came back to its earlier value in 1997 (Fig. 10).

Despite the existence of several fault branches which required appropriate monitoring, the site number 5 (the Chinyuan river) is of special value because the geodetic surveys were never interrupted. The upper, and most important fault, locally follows a nearly horizontal line of drainage pipes in the wall, because of the mechanical weakness making fracture development and propagation easier. The concrete walls of the Chihshang river were built in 1984–1985; the age of fracturing is not accurately known; fractures already existed in 1988. Total displacement data were collected from 1991 to 1997. In addition, surveys involving more accurate techniques (such as nail networks) started in 1992. Because the intermediate and lower fault branches not only interfere due to their small spacing (less than 10 m), but also cross the walls in a sharp

bend of the river, complex fracturing and deformation affects the curved walls, resulting in less accurate determinations.

As mentioned earlier, the record of fault displacement obtained at Chinyuan also illustrates the development of a new reverse fault zone (the middle fault) below the main one, at a larger distance (about 40 m downstream) than in site 3. This middle fault probably appeared in late 1989–early 1990. In addition, minor fracturing about 200 m downstream suggests an incipient stage for the nucleation of a third, lower fault. Site 5 thus illustrates the present-day in-sequence shift of reverse faulting, with decreasing activity on the upper thrusts, and increasing activity on the lower ones.

The estimates of the total motion at Chinyuan are partly influenced by the poor record for the middle fault segment, despite an excellent accuracy for the upper fault. However, accurate estimates of motion on the middle fault could be made during the last few years in the bottom of the river. These new results are compatible with a rather stable velocity of horizontal shortening, 1.9 cm /yr, resulting in a total displacement of about 21 cm in about 9.5 years (1988–1997). As for the other sites, the velocity slightly decreased in 1993.

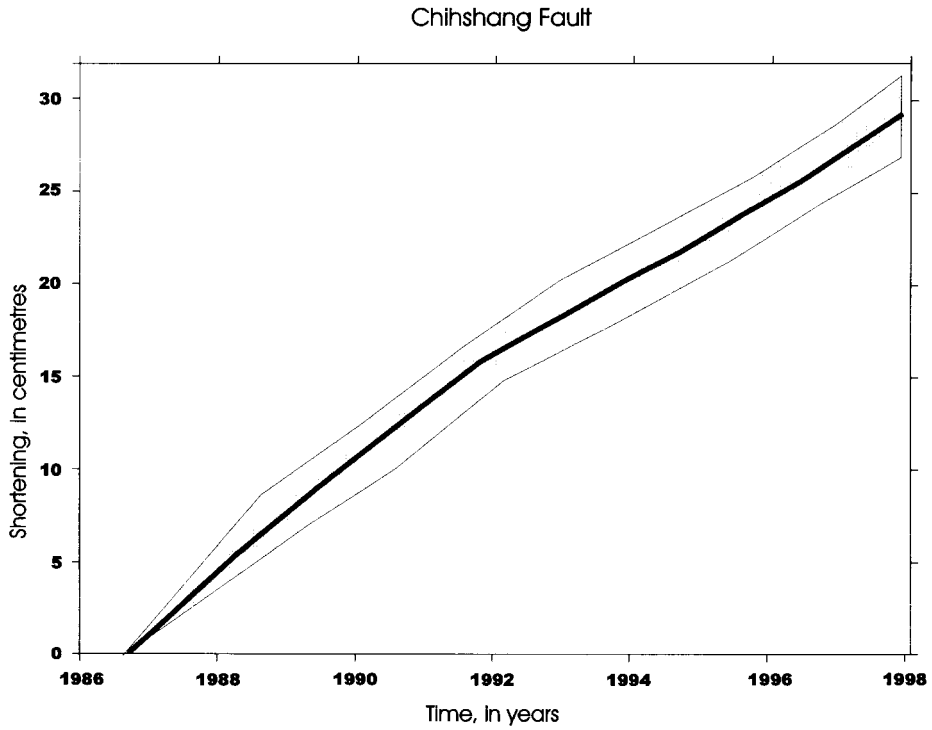

Fig. 14. A summary of the evolution of shortening across the Chihshang Fault, 1986–1997. Cumulative displacement as ordinate, time as abscissa. Shortening measured along the trend of relative motion vector. Average shortening as thick line, error domain shaded.

7.2. Slip variations through time along the Chihshang Fault

A striking character of Fig. 10 lies in the generally similar slopes of the curves independently obtained at the four sites. It appears that local variations are minor and that the average local velocity of horizontal shortening ranges between 2.2 and 2.9 cm/yr. Most local velocities are closer to the lowest bound, whereas the only velocity close to the highest bound is that of site 3; as a consequence, these results suggest an average velocity of 2.4 ± 0.2 cm/yr on average for the Chihshang Fault during the period 1986–1997 (Fig. 14). This rate represents a total shortening of 29 ± 2 cm in nearly 12 years.

In more detail, variations in slip rate have certainly occurred during the period 1986–1997. A decrease in velocity took place in late 1993 and 1994 at sites 3, 4 and 5 (Fig. 10). Because estimates were done independently at these sites, this variation is significant, although it was limited (as far as annual surveys may reveal). Some of the variations in time are strictly local. For instance, at site 3, a minor increase in velocity coincided with the development of the lower fault beneath the older one in 1989–1990 (Angelier et al., 1997). Such local variations probably result from strain accumulations and elastic responses when fracture patterns are changing. That they do not reflect any change in the general behaviour of the Chihshang Fault clearly results from the lack of correlation between the velocity variations recorded at different sites.

In contrast, variations in slip rate recorded simultaneously at different sites are significant at the scale of the entire active segment of the Chihshang Fault. This is the case for the consistent decrease in velocity recorded at the three sites available for annual surveys in 1993–1994. For a period of 11.5 months, the shortening was 1.7, 1.7 and 1.5 at sites 3, 4 and 5 respectively, indicating an average velocity of 1.7 cm/yr. This velocity represents about one half of that measured for the preceding twelve months at the same sites (shortenings of 4 , 2.1 and 3.4 cm respectively, i.e., an average velocity of 3.2 cm/yr.). Considering the average velocity of 2.2 cm/yr determined for longer periods (Figs. 10 and 14), the relative decrease was 25% in 1993–1994, a value that falls outside the range of uncertainties and must therefore be regarded as geologically significant (note that there was no technical reason for errors to occur simultaneously at all sites).

Fault slip continued after this 1993–1994 event at the same average velocity as before, so that this phenomenon did not reveal any persisting decrease in the activity of the Chihshang Fault. Such a persisting decrease would have meant that compressional strain was accumulating somewhere in the Chishang region, implying increasing earthquake hazard along the Chihshang segment of the Longitudinal Valley Fault Zone. This also explains why the authors of this paper are presently developing more extensive and permanent monitoring of the displacement on the Chihshang Fault.

The compilation of all the results finally indicates that the average velocity (Fig. 14) generally decreased from about 16 cm in less than 6 years before 1992 (almost 3 cm/yr) to about 13 cm in less in 6 years in the period 1992–1997 (2.2 cm/yr). It should be noticed, however, that the latter determination is tightly constrained by numerous accurate measurements, whereas the former is far from being accurately determined. This high value corresponds to a period with much less data collection and lower technical accuracy. Furthermore, the average value obtained heavily depends on the interpolations made at sites 3

and 5 (Fig. 10). The most significant estimates of the fault slip rate are those computed for the last seven years (1991–1997), which give a value of 2.2 cm/yr. Taking uncertainties into account, this slip rate can be considered to be constant for this whole period (Fig. 14).

8. Role of the Longitudinal Valley Fault in the oregon

By comparing the results obtained at both the outcrop scale (this study) and the regional scale (the Taiwan GPS network), it is possible to give a better account of the kinematics and mechanics of the Chihshang Fault, part of the Longitudinal Valley Fault Zone, in the active collision belt of Taiwan (Fig. 1).

8.1. The present-day plate boundary

As shown before, the results of our local surveys along the active Chihshang Fault are generally compatible with the results previously obtained in the same region, although the techniques, the scales and the time spans considered differ. Three geodetic networks had been established across the Longitudinal Valley at Chihshang, Yuli and Juisui, with segment lengths in the range 1–12 km and total distances in the range 5–15 km (Fig. 2). The results for the period 1983–1988 (Yu and Liu, 1989 and Yu et al., 1990) indicate maximum shortening along the N132°E (N48°W) direction. Later analyses of the same data with a discontinuity model (Lee and Angelier, 1993) indicate convergence along the directions N146°E (N34°W) for the Chihshang network and N141°E (N39°W) on average for the three networks. The average velocity computed is 2.1 cm/yr. The consistency between the three motion vectors calculated over a distance of 63 km along the Longitudinal Valley Fault Zone suggests that these determinations reliably reflect the kinematic behaviour of the Yuli segment of the Longitudinal Valley Fault Zone.

In terms of the orientation of relative displacement, there is a good consistency between the N34–39°W trends obtained from these geodetic studies (Fig. 2) and the averaged N40°W trend that we obtained for sites 3, 4 and 5, despite local variations (from N24°W at site 3 to N61°W at site 4). In terms of velocity, the values obtained are identical within the range of uncertainties (2.1 and 2.2 cm/yr, respectively). We infer that the 3-D pattern of slip on the Chihshang Fault, shown in Fig. 6, equally applies to the geodetic data from trilateration networks and to averaged local measurements (our in-situ estimates provides velocities 5% higher for all the components of slip, a difference that is not significant).

Incidentally, the data extracted from the Taiwan GPS network (Yu and Chen, 1994; Yu et al., 1995 and 1997) and discussed earlier in this paper (Fig. 3) yield a very similar direction of relative displacement (N37°W) but a significantly larger velocity (3.1 cm/yr). This difference cannot be accounted for by uncertainties; it probably reflects the presence of deformation occurring on the edge of the Longitudinal Valley. Whatever the explanation, the activity of the Chihshang Fault accounts for about one fourth (24%), and that of the Longitudinal Valley Fault Zone for more than one third (37%), of the total shortening between the Luzon Arc and the South China shelf, as measured along the N54°W direction of plate convergence. An interesting aspect of our study is that 100% of the total horizontal shortening near Chihshang

between the western foot of the Coastal Range and the eastern foot of the Central Range (2.2 cm/yr), occurs across a single, narrow fault zone. This provides a good example of shear concentration in an oblique collision zone (Angelier et al., 1997).

As discussed earlier in this paper, based on GPS data (Fig. 3), the contribution of the Longitudinal Valley Fault Zone to the total deformation of the Taiwan collision zone reaches 2.5 cm/yr, that is 32% for across-strike shortening, and 1.8 cm/yr, that is 80% for along-strike left-lateral displacement. In other words, the tectonic activity of the Longitudinal Valley Fault Zone accounts for four fifths of the total belt-parallel shear, whereas it accommodates one third of the belt-perpendicular shortening.

The distinct-element numerical modelling analyses presented by Hu et al. (1997) show that this kinematic behaviour is well accounted for by the strain-stress partitioning resulting from the mechanical weakness of the Longitudinal Valley boundary, where more left-lateral slip takes place relative to other deforming zones of the collision belt. Although there are several major zones of weakness across the collision belt, none of them has the kinematic importance of the Longitudinal Valley Fault Zone and its potential to induce large mechanical decoupling across the Taiwan collision zone. This strongly supports the choice of the Longitudinal Valley Fault Zone as the present-day plate boundary (Fig. 1).

8.2. A major suture zone of the late Cenozoic

Was the Longitudinal Valley Fault a major boundary in the past? The answer is certainly positive in view of the major differences between the eastern side (the Coastal Range, a deformed northern segment of the Luzon Arc) and the western one (the Central Range, a deformed and metamorphosed domain of the Eurasian margin). Also, the present-day Chihshang Fault generally follows the elongated zone of the Lichi Mélange, a highly deformed and sheared formation which in most cases crops out as a narrow tectonic unit between the Longitudinal Valley and the Coastal Range.

The Lichi Mélange consists of heavily sheared Pliocene marine clays containing numerous blocks of the East Taiwan ophiolite and Miocene sandstones. The Miocene calc-alkaline volcanic formations of the Coastal Range are overlain by the thick marine flysch-like sediments of the Takangkou formation, Plio-Pleistocene in age. The complex stratigraphic and tectonic relationships between the Pliocene Lichi Mélange and this Takangkou formation suggest that the Lichi Mélange developed as a result of gravity sliding and tectonic shearing on the western edge of a large Takangkou sedimentary basin, prior to the final collision stage of Taiwan. Whatever its origin (the western Philippine Sea plate, or an oceanic domain of the Eurasian plate such as for the South China Sea), the presence of the East Taiwan ophiolite in the Lichi Mélange highlights the importance of the Longitudinal Valley of eastern Taiwan, not only as the present-day plate boundary (Fig. 1), but also as a major suture zone resulting from the late Cenozoic history of plate convergence.

It is important to mention, however, that the Longitudinal Valley Fault does not strictly follows the major suture zone. Accordingly, the Longitudinal Valley Fault Zone was not a fixed boundary during the late Quaternary. To the north, between 23.6°N and 24°N, the active fault does not follow the geological suture zone of the Longitudinal Valley that separates the Coastal Range and the Central Range of Taiwan. The northern segment of the active fault

crosses obliquely the Coastal Range from the Longitudinal Valley to the eastern coast, and merges into the offshore active tectonic zone that separates the Taiwan collision belt and the westernmost portion of the Ryukyu subduction zone (Angelier et al., 1995). In other words, most of the active Longitudinal Valley Fault coincides with the late Cenozoic major suture zone, as well as with the late Quaternary and present-day topographic expression of the Longitudinal Valley; but this is true only south of 23.6°N. One may therefore infer that during the late Quaternary, the northernmost portion of the Longitudinal Valley Fault was abandoned as a site of reverse-sinistral shear concentration (which jumped eastwards). In contrast, to the south it remained, and still is, the major plate boundary including the active Chihshang Fault.

8.3. Distribution of Quaternary compression

Tectonic analyses of quaternary faulting were carried out throughout the Coastal Range, east of the Longitudinal Valley Fault Zone (Barrier and Angelier, 1986). They revealed widespread compression along N90°E to N140°E trends (for 90% of the data), with numerous compressional trends around N120°E (25% of the data). Studies of brittle deformation were carried out in the Pinanshan conglomerates, Quaternary in age, which represent the earliest alluvial formations of the Longitudinal Valley. They revealed compression trending N100°E in the conglomerates to N140°E on the eastern side of the valley (Barrier et al., 1982). This situation is of interest because in this particular area of the Longitudinal Valley Fault Zone strain and stress partitioning occurs between two branches of the active fault. The western branch principally behaves as a thrust, whereas most of the strike-slip component (left-lateral) concentrates along the eastern branch. This partitioning has been analysed by Lee et al. (1998), who re-interpreted the geodetic data available for the Pinanshan area.

At the scale of the entire Taiwan collision belt, the directions of compression related to quaternary shortening across the fold-and-thrust belt and the general direction of the plate convergence are similar. The trajectories of maximum compressive stress are fan-shaped, as revealed by reconstructions of the Quaternary stress field (Angelier et al., 1986). For the present-day seismic activity, the inversion of the focal mechanisms of earthquakes led to similar conclusions (Yeh et al., 1991). The average regional trend of quaternary compression is N122°E (N58°W) for central Taiwan; however, regional variations in trend result in deviations as large as 40° clockwise (to the north) and 20° counterclockwise (to the south). Near Chihshang, strain analyses in trilateration networks revealed N132°E (N48°W) shortening across the Longitudinal Valley Fault Zone. In comparison with the average directions of compression derived from fault-slip studies across the whole collision zone of central Taiwan, the deviation average 10° clockwise. This deviation of the principal strain-stress axes resembles that already noticed for displacement vectors.

This brings additional support to the interpretation of the Longitudinal Valley Fault Zone as a major site of mechanical weakness and tectonic partitioning. Whereas the finite-element numerical modelling allowed to check the mechanical likelihood of the overall perturbations at the scale of the orogen, in terms of the relationships between internal deformation and boundary kinematic conditions (Hu et al., 1996), the distinct-element modelling (Hu et al.,

1997) allowed more precise evaluation of the role of the major discontinuities like the Longitudinal Valley Fault and the front thrusts.

9. Conclusions

The study presented in this paper shows that reliable estimates of active fault displacement can be obtained not only in desertic areas, but also in tropical countries provided that severe requirements are fulfilled. Of major interest are the variations of slip rates with time, because they may have strong influence in terms of earthquake hazard. Our local surveys provided an accurate record of the kinematic evolution of the Chihshang Fault, and of the main slip variations analysed accurately during a time window of about twelve years. The relative displacement vector of the active Chihshang Fault trends N40°W on average, with a velocity of 2.2 cm/yr. The determinations of the three components of relative displacement of the Chihshang Fault (Fig. 6) highlight its role as a site of oblique motion, thrust and left-lateral in type. The excellent fit between our local determinations and those derived from the 6 km-wide Chihshang geodetic network across the Longitudinal Valley demonstrates that near 23°N the entire shortening across the Longitudinal Valley concentrates on the Chihshang Fault. The data obtained from ten GPS stations on both sides of the valley reveal a higher relative velocity, possibly because they involve additional shortening on valley sides.

As far as the annual surveying from 1990 to 1997 is concerned, the reconstruction of the slip velocity shows that variations are quite small, albeit some are marginally significant (Figs. 10 and 14), as the one which occurred in 1993 across the Chihshang Fault. Unfortunately, this decrease slip velocity was followed by human wall destruction at two major sites, resulting in the loss of network and the impossibility to obtain reliable estimates for the next few years. However, good quality surveys carried out at the remaining two sites during the following three years showed that, after this decrease, the slip velocity on the Chihshang Fault had come back to the same level as before.

At the present, fault creeping behaviour clearly prevails on the Chihshang Fault zone, where no large earthquake has occurred since 1951 and earthquake activity remains minor. Despite the absence of accurate records at that time, the earthquake crisis in 1951 probably closed a stage of fault locking and compressional stress accumulation. It is likely that the 1951 earthquakes also initiated the present-day creeping period. A new major decrease in fault slip velocity would probably announce a new stage of fault locking and accumulating compressive stress, and hence an increasing earthquake hazard. For this reason, we paid particular attention to the 1993 decrease in slip velocity, which subsequently revealed to be only temporary.

Following the evolution of active fault slip in detail appeared to be an important target. This is because had the decrease in non-seismic slip velocity continued, the accumulation of compressional strain would probably have occurred in the area as a result of the continuing convergence, involving an increase in earthquake hazard. Because they give information on the total strain over large areas, the studies carried out at the regional scale have less potential than local analyses to allow detection of frictional variations on the active fault. The local evolution of earthquake hazard with time heavily depends on these variations. Whether the

local fault behaviour remains mechanically weak, with low friction (as it was the case for the Chihshang Fault during the period 1986–1997), or gradually changes towards a locking situation, is a crucial question. Part of the answer can be obtained through local surveys of the type discussed herein. For these reasons, a more permanent surveying of the Chihshang Fault has been set up in 1998 at two key sites (the Tapo school and the Chinyuan channel).

Acknowledgements

This work was carried out within the frame of the cooperation France–Taiwan in Earth Sciences, supported by the Institut Français à Taipei (I.F.T.) and the National Science Council of Taiwan (N.S.C.). Supports from the University Pierre-et-Marie Curie (Paris), the Central Geological Survey of Taiwan and the Institute of Earth Sciences, Academia Sinica (Taipei) are gratefully acknowledged. The generous help of Mr. Jiang Kuo-Chang, retired Professor in Taitung, Mr. Chang Chen-Hsiung, Director of the Tapo School, and others, was deeply appreciated during our field surveys. May also Dr. G. Cello, who helped us to present these results at the International Workshop "The Resolution of Geological Analysis and Models for Earthquake Faulting Studies" (held in Camerino, Italy) and publish this paper, receive our sincere thanks.

References

Angelier, J., 1986. Geodynamics of the Eurasia — Philippine Sea Plate boundary: Preface. Tectonophysics 125 (13), 9–10.

Angelier, J., Barrier, E., Chu, H-T., 1986. Plate collision and paleostress trajectories in a fold-thrust belt: the Foothills of Taiwan. Tectonophysics 125, 161–178.

Angelier, J., Bergerat, F., Chu, H.T., Lee, T.Q., 1990. Tectonic-paleomagnetic analyses and the evolution of a curved collision belt: the Hsüeshan Range, northern Taiwan. Tectonophysics 183, 77–96.

Angelier, J., Lee, J-C., Chu, H-T., Lu, C-Y., Fournier, M., Hu, J-C., Lin, N-T., Deffontaines, B., Delcaillau, B., Lacombe, O., Lee, T-Q. 1995. Crustal extension in an active orogen: Taiwan. ACT (Active Collision of Taiwan) Intern. Conf., Extended Abstracts, Tsien H.-H. ed., Geological Society of China Special Publication, Taipei, Taiwan, pp. 25–32.

Angelier, J., Chu, H-T., Lee, J-C., 1997. Shear concentration in a collision zone: kinematics of the Chihshang Fault as revealed by outcrop-scale quantification of active faulting, Longitudinal Valley, eastern Taiwan. Tectonophysics 274, 117–143.

Barrier, E., Angelier, J., Chu, H-T., Teng, L-S., 1982. Tectonic analysis of compressional structure in an active collision zone: the deformation of the Pinanshan Conglomerates, eastern Taiwan. Proceedings Geological Society of China 25, 123–138.

Barrier, E., Angelier, J., 1986. Active collision in eastern Taiwan: the Coastal Range. Tectonophysics 125, 39–72.

Barrier, E., Chu, H-T., 1984. Field trip guide to the Longitudinal Valley and the Coastal Range in eastern Taiwan. In: Field Guidebook for the Sino-French Colloquium on Geodynamics of Eurasia-Philippine Sea Plate Boundary, Taipei, Taiwan, pp. 27–49.

Bonilla, M.G., 1977. Summary of Quaternary faulting and elevation changes in Taiwan. Memoir of the Geological Society of China 2, 43–56.

Chu, H-T., Lee, J-C., Angelier, J. 1994. Non-seismic rupture of the Tapo and the Chinyuan area on the southern segment of the Huatung Longitudinal Valley Fault, Eastern Taiwan. Geological Society of China, Annual Meeting, Taipei, 25–26 March 1994, Collected Abstracts, 1–5.

Ho, C-S., 1986. A synthesis of the geologic evolution of Taiwan. Tectonophysics 125, 1–16.
Hsu, T-L., 1962. Recent faulting in the Longitudinal Valley of eastern Taiwan. Memoir of the Geological Society of China 1, 95–102.
Hu, J-C., Angelier, J., Lee, J-C., Chu, H-T., Byrne, D., 1996. Kinematics of convergence, deformation and stress distribution in the Taiwan collision area: 2-D finite-element numerical modelling. Tectonophysics 255, 243–268.
Hu, J-C., Angelier, J., Yu, S-B., 1997. An interpretation of the active deformation of southern Taiwan based on numerical simulation and GPS studies. Tectonophysics 274 (13), 145–169.
Lee, J-C., 1994. Structure et déformation active d'un orogéne: Taiwan. Mémoires des Sciences de la Terre 94 (17), 281 (Université Pierre et Marie Curie, Paris).
Lee, J-C., Angelier, J., 1993. Localisation des déformations actives et traitement des données géodésiques: l'exemple de la faille de la Vallée Longitudinale, Taiwan. Bulletin de la Société Géologique de France 164 (4), 533–570.
Lee, J-C., Angelier, J., Chu, H-T., Yu, S-B., Hu, J-C., 1998. Plate-boundary strain partitioning along the sinistral collision suture of the Philippine and Eurasian plates: analysis of geodetic data and geological observation in southeastern Taiwan. Tectonics 17 (6), 859–871.
Seno, T., 1977. The instantaneous rotation vector of the Philippine Sea plate relative to the Eurasian plate. Tectonophysics 42, 209–226.
Seno, T., Stein, S., Gripp, A.E., 1993. A model for the motion of the Philippine Sea plate consistent with NUVEL-1 and geological data. Journal of Geophysical Research 98, 17941–17948.
Tsai, Y-B., 1986. Seismotectonics of Taiwan. Tectonophysics 125, 17–37.
Yeh, Y-H., Barrier, E., Lin, C-H., Angelier, J., 1991. Stress tensor analysis in the Taiwan area from focal mechanisms of earthquakes. Tectonophysics 200, 267–280.
York, J-E., 1976. Quaternary faulting in eastern Taiwan. Bulletin of the Central Geological Survey of Taiwan 25, 63–72.
Yu, S-B., Jackson, D-D., Yu, G-K., Liu, C-C., 1990. Dislocation model for crustal deformation in the Longitudinal Valley area, Eastern Taiwan. Tectonophysics 183, 97–109.
Yu, S-B., Liu, C-C., 1989. Fault creep on the central segment of the Longitudinal Valley Fault, Eastern Taiwan. Proceedings of the Geological Society of China 32 (3), 209–231.
Yu, S-B., Chen, H-Y., Kuo, L-C. 1995. Velocity field of GPS Stations in the Taiwan area. ACT (Active Collision of Taiwan) International Conference, Extended Abstracts, Tsien H.-H. ed., Geological Society of China Special Publication, Taipei, Taiwan, pp. 317–327.
Yu, S-B., Chen, H-Y., Kuo, L-C., 1997. Velocity field of GPS Stations in the Taiwan area. Tectonophysics 274 (13), 41–59.
Yu, S-B., Chen, H-Y., 1994. Global Positioning System measurements of crustal deformation in the Taiwan arc-continent collision zone. Terrestrial, Atmospheric and Oceanic Sciences 5, 477–498.
Yu, S-B., Tsai, Y-B., 1982. A study of microseismicity and crustal deformation of the Kuangfu-Fuli area in eastern Taiwan. Bulletin of the Institute of Earth Sciences, Academia Sinica 2, 1–18.